UNCLASSIFIED

AD NUMBER
AD871425
LIMITATION CHANGES
TO: **Approved for public release; distribution is unlimited.**
FROM: **Distribution authorized to U.S. Gov't. agencies and their contractors; Critical Technology; MAR 1970. Other requests shall be referred to U.S. Army Aviation Materiel Laboratories, Fort Eustis, VA 23604. This document contains export-controlled technical data.**
AUTHORITY
USAAMRDL ltr, 23 Jun 1971

THIS PAGE IS UNCLASSIFIED

AD 871425

AD No. ____
DDC FILE COPY

AD

USAAVLABS TECHNICAL REPORT 70-9

ON THE OPTIMUM PROPORTIONING OF STIFFENED CIRCULAR CURVED PLATES AND SHELLS FOR AXIAL COMPRESSION LOADING

By

E. Meller
J. Mayers

March 1970

U. S. ARMY AVIATION MATERIEL LABORATORIES
FORT EUSTIS, VIRGINIA

CONTRACT DAAJ02-68-C-0035
STANFORD UNIVERSITY
STANFORD, CALIFORNIA

This document is subject to special export controls, and each transmittal to foreign governments or foreign nationals may be made only with prior approval of US Army Aviation Materiel Laboratories, Fort Eustis, Virginia 23604.

U S ARMY MATERIEL COMMAND

DDC
JUL 10 1970
B

72

Disclaimers

The findings in this report are not to be construed as an official Department of the Army position unless so designated by other authorized documents.

When Government drawings, specifications, or other data are used for any purpose other than in connection with a definitely related Government procurement operation, the United States Government thereby incurs no responsibility nor any obligation whatsoever; and the fact that the Government may have formulated, furnished, or in any way supplied the said drawings, specifications, or other data is not to be regarded by implication or otherwise as in any manner licensing the holder or any other person or corporation, or conveying any rights or permission, to manufacture, use, or sell any patented invention that may in any way be related thereto.

Disposition Instructions

Destroy this report when no longer needed. Do not return it to the originator.

ACCESSION for
CFSTI WHITE SECTION
DDC BUFF SECTION
UNANNOUNCED
JUSTIFICATION
DISTRIBUTION/AVAILABILITY CODES
DIST. AVAIL. and/or SPECIAL

DEPARTMENT OF THE ARMY
HEADQUARTERS US ARMY AVIATION MATERIEL LABORATORIES
FORT EUSTIS, VIRGINIA 23604

This program was carried out under Contract DAAJ02-68-C-0035 with Stanford University.

The research was directed to the development of techniques and criteria for designing stringers and riugs for curved plates and shells of minimum weight to obtain maximum initial buckling near the classical buckling load.

The report haa been reviewed by the U.S. Army Aviation Materiel Laboratories and is considered to be technically sound. It is published for the exchange of information and the stimulation of future research.

Task 1F162204A17002
Contract DAAJ02-68-C-0035
USAAVLABS Technical Report 70-9
March 1970

ON THE OPTIMUM PROPORTIONING OF STIFFENED CIRCULAR CURVED PLATES AND SHELLS FOR AXIAL COMPRESSION LOADING

Final Report

By

E. Meller
J. Mayers

Prepared by
Department of Aeronautics and Astronautics
Stanford University
Stanford, California

for

U. S. ARMY AVIATION MATERIEL LABORATORIES
FORT EUSTIS, VIRGINIA

This document is subject to special export controls, and each transmittal to foreign governments or foreign nationals may be made only with prior approval of U. S. Army Aviation Materiel Laboratories, Fort Eustis, Virginia 23604.

SUMMARY

An investigation is undertaken to (1) reevaluate the elastic theory results obtained by previous investigators for both perfect and initially imperfect, axially compressed circular cylindrical shells, (2) develop new elastic stability results describing the postbuckling behavior of curved plates, and (3) present criteria based, in part, upon the curved plate results which can be used to size and locate stringers and rings such that the initial buckling load will occur in the neighborhood of the classical buckling load for a cylinder representing a minimized-weight design.

FOREWORD

The work reported herein constitutes a portion of a continuing effort being undertaken at Stanford University for the U. S. Army Aviation Materiel Laboratories under Contract DAAJ02-68-C-0035 (Task 1F162204A17002) to establish accurate theoretical prediction capability for the static and dynamic behavior of aircraft structural components utilizing both conventional and unconventional materials. Predecessor contracts supported investigations which led, in part, to the results presented in references 16, 19, 24, and 25.

TABLE OF CONTENTS

	Page
SUMMARY	iii
FOREWORD	v
LIST OF ILLUSTRATIONS	viii
LIST OF SYMBOLS	ix
INTRODUCTION	1
GENERAL THEORY	4
Strain-Displacement Relations	4
Stress-Strain Relations	5
Potential Energy	6
Alternate Form of Total Potential Energy Functional	7
METHOD OF SOLUTION	11
Circular Cylindrical Shell	11
Circularly Curved Plate	14
RESULTS AND DISCUSSION	17
Circular Cylindrical Shell	17
Circularly Curved Plate	24
CONCLUDING REMARKS	29
LITERATURE CITED	42
APPENDIXES	
I. Development of Governing Equations and Boundary Conditions	46
II. Solution of Compatibility Equation	53
III. Solution of Curved-Plate Problem	58
DISTRIBUTION	61

LIST OF ILLUSTRATIONS

Figure		Page
1	Geometry and Sign Convention for Curved Plate and Complete Shell	31
2	Average Stress-Unit End Shortening Curves (Present Analysis and Reference 13)	32
3	Average Stress-Unit End Shortening Curves (Present Analysis and Reference 8)	33
4	Average Stress-Unit End Shortening Curve for Kempner Radial Deflection Function (Present Analysis Digital Computer Solution and Desk Calculator Points Obtained in Reference 13)	34
5	Average Stress-Unit End Shortening Curves for Perfect and Imperfect Shells (Comparison of Present Analysis Solutions With Those of Reference 12)	35
6	Average Stress-Unit End Shortening Curves for Flat and Curved Plates Covering the Range $0 \leq Z \leq \infty$	36
7	Average Stress-Unit End Shortening Curve for Modified-Kempner Radial Deflection Function ($A_{02} = 0$)	37
8	Variation of Radial Deflection Pattern Amplitudes A_{11}, A_{20}, and A_{02} With Unit End Shortening for Present Analysis Solution Corresponding to Kempner Deflection Function	38
9	Variation of Radial Deflection Pattern Wave Parameters μ and η With Unit End Shortening for Present Analysis Solution Corresponding to Kempner Deflection Function	39
10	Effect of Lightweight Longitudinal Stiffeners in Preventing Catastrophic Snap-Through Buckling Into a Yoshimura Pattern	40
11	Physical Properties of Stiffened Shell Used as a Basis for Optimizing Procedure	41

LIST OF SYMBOLS

A_{ij}	nondimensionalized displacement parameter
A_{ij}^{0}	nondimensionalized initial deviation displacement parameter
A_{ij}^{*}	nondimensionalized initial deviation displacement-growth parameter
a, a_0	circumferential half-wavelength parameters, 1/in.
b	width of curved plate, in.
C	empirical constant
D	bending rigidity, lb-in.
E	Young's modulus, lb/in.^{2}
e	unit end shortening, in./in.
F	Airy stress function, lb
L	length of either circular cylindrical shell or curved plate, in.
M_x, M_y	bending moments per unit length in x- and y-directions, respectively, lb
M_{xy}	twisting moment per unit length, lb
N	number of buckle half-waves in the circumferential direction for curved plate
N_x, N_y	total loads per unit length in x- and y-directions, respectively, lb/in.
N_{xy}	total shear load per unit length in middle surface, lb/in.
R	mean radius of circular cylindrical shell or curved plate, in.
t	thickness of either circular cylindrical shell or curved plate, in.
U	total strain energy of stretching and bending, lb-in.
u,v,w	displacements of point on middle surface of either circular cylindrical shell or curved plate in x-, y-, and z-directions, respectively, in.

w_0, w_T	initial deviation and total displacement, respectively, in z-direction, in.
x, y, z	cylinder and curved plate coordinates, in.
Z	nondimensional curvature parameter
α, β, γ	constants defined in Appendix III
γ_{xy}	total shearing strain in middle surface, in./in.
Δ	constant defined in Appendix III
δ_{1N}	Kronecker delta
ϵ_x, ϵ_y	total strains in x-, and y-directions, respectively, in./in.
η, η_0	nondimensional wave-number parameters; constant in equation (28)
λ_x, λ_y	buckle half-wavelengths of either cylinder or curved plate in axial and circumferential directions, respectively, in.
$\lambda_{x_0}, \lambda_{y_0}$	buckle half-wavelengths of initial deviation of either cylinder or curved plate in axial and circumferential directions, respectively, in.
μ, μ_0	buckle aspect ratios
ν	Poisson's ratio
σ	average compressive stress, lb/in.^{2}
σ_x, σ_y	total stresses in x- and y-directions, respectively lb/in.^{2}
τ_{xy}	total shear stress in middle surface, lb/in.^{2}
ϕ, ψ	constants defined in Appendix III

OPERATOR SYMBOLS

$\nabla^4(\ )$	defined by $(\ )_{,xxxx} + 2(\ )_{,xxyy} + (\ )_{,yyyy}$
$\nabla^{-4}(\ )$	defined by $\nabla^4\nabla^{-4}(\ ) = (\ )$

SUPERSCRIPTS

0	denotes extensional strain
1	denotes bending strain

w_0, w_T	initial deviation and total displacement, respectively, in z-direction, in.
x, y, z	cylinder and curved plate coordinates, in.
Z	nondimensional curvature parameter
α, β, γ	constants defined in Appendix III
γ_{xy}	total shearing strain in middle surface, in./in.
Δ	constant defined in Appendix III
δ_{1N}	Kronecker delta
ϵ_x, ϵ_y	total strains in x-, and y-directions, respectively, in./in.
η, η_0	nondimensional wave-number parameters; constant in equation (28)
λ_x, λ_y	buckle half-wavelengths of either cylinder or curved plate in axial and circumferential directions, respectively, in.
$\lambda_{x_0}, \lambda_{y_0}$	buckle half-wavelengths of initial deviation of either cylinder or curved plate in axial and circumferential directions, respectively, in.
μ, μ_0	buckle aspect ratios
ν	Poisson's ratio
σ	average compressive stress, lb/in.^{2}
σ_x, σ_y	total stresses in x- and y-directions, respectively lb/in.^{2}
τ_{xy}	total shear stress in middle surface, lb/in.^{2}
ϕ, ψ	constants defined in Appendix III

OPERATOR SYMBOLS

$\nabla^4(\ )$	defined by $(\ )_{,xxxx} + 2(\ )_{,xxyy} + (\ )_{,yyyy}$
$\nabla^{-4}(\ )$	defined by $\nabla^4\nabla^{-4}(\ ) = (\ )$

SUPERSCRIPTS

0	denotes extensional strain
1	denotes bending strain

approaches zero. Meanwhile, by utilizing a more exact set of strain-displacement relations than von Kármán-Donnell, Mayers and Rehfield, in 1965, had obtained radius-to-thickness-dependent, load-end shortening curves for the Kempner deflected shape and showed that the von Kármán-Donnell-theory solution obtained by Kempner is reached only as the thickness-to-radius ratio of the cylinder approaches zero. As is demonstrated in reference 15, the deflected shape of the converged potential energy solution of the von Kármán-Donnell equations approaches the developable-surface shape derived by Yoshimura.[17] Thus, in view of the findings of Hoff et al.[15] and Mayers and Rehfield,[16] it became evident that elastic analysis postbuckling curves for perfect shells were of no practical significance. Attention was then turned to the elastic behavior of imperfect, axially compressed, circular cylindrical shells in attempts to more accurately predict the initial buckling or maximum load. The major effort in this area is included, also, in the work of Madsen and Hoff reported in reference 12.

However, despite the extensive and important information concerning the elastic stability and postbuckling behavior of axially compressed cylinders included in references 1-17, there is still no theoretical analysis which will predict the initial elastic buckling load of a practically fabricated, thin, axially compressed cylinder. More important, since pure monocoque shells are the exception rather than the rule in shells designed for compression loading, there is no theoretical analysis which can (1) predict the initial buckling load of a thin stiffened cylinder even if the behavior is elastic and (2) provide design criteria whereby the stiffened cylinder will reflect an optimized design.

It is the purpose of the present investigation to (1) reevaluate the elastic theory results obtained by previous investigators for both perfect and initially imperfect, axially compressed circular cylindrical shells, (2) develop new elastic stability results describing the postbuckling behavior of curved plates, and (3) present criteria based in part upon the curved plate results which can size and locate stringers and rings such that the initial buckling load will occur in the

neighborhood of the classical buckling load for a cylinder representing a minimized-weight design. All three objectives have been met; the findings are presented in the form of equations and graphs. The results of the analyses and the computations are presented in the body of the report, and the details of the analyses and computational procedures are given in a series of appendixes.

GENERAL THEORY

STRAIN-DISPLACEMENT RELATIONS

The strain-displacement relations used herein are the small strain, large displacements-moderate rotations set derived by Donnell with modifications to account for initial deviations from uniform circularity along the shell length, with w_0 denoting the initial imperfection shape, w denoting the additional deflection due to bending of the shell during load application, and w_T denoting the sum of w_0 and w; that is,

$$w_T = w_0 + w \tag{1}$$

The strain-displacement equations for the middle surface of the shell (see Figure 1) are

$$\left.\begin{aligned}
\epsilon_x^0 &= u_{,x} + \frac{1}{2}\left(w_{T,x}^2 - w_{0,x}^2\right) \\
\epsilon_y^0 &= v_{,y} + \frac{1}{2}\left(w_{T,y}^2 - w_{0,y}^2\right) - \frac{(w_T - w_0)}{R} \\
\gamma_{xy}^0 &= u_{,y} + v_{,x} + w_{T,x} w_{T,y} - w_{0,x} w_{0,y}
\end{aligned}\right\} \tag{2}$$

In view of equation (1), equations (2) are rewritten as

$$\left.\begin{aligned}
\epsilon_x^0 &= u_{,x} + \frac{1}{2} w_{,x}^2 + w_{,x} w_{0,x} \\
\epsilon_y^0 &= v_{,y} + \frac{1}{2} w_{,y}^2 + w_{,y} w_{0,y} - \frac{w}{R} \\
\gamma_{xy}^0 &= u_{,y} + v_{,x} + w_{,x} w_{,y} + w_{0,x} w_{,y} + w_{,x} w_{0,y}
\end{aligned}\right\} \tag{3}$$

The bending strains are

$$\left.\begin{aligned} \epsilon_x^1 &= -zw_{,xx} \\ \epsilon_y^1 &= -zw_{,yy} \\ \gamma_{xy}^1 &= -2zw_{,xy} \end{aligned}\right\} (4)$$

Thus, the total strains, equations (3) plus equations (4), are

$$\left.\begin{aligned} \epsilon_x &= \epsilon_x^0 + \epsilon_x^1 = u_{,x} + \frac{1}{2} w_{,x}^2 + w_{,x}w_{0,x} - zw_{,xx} \\ \epsilon_y &= \epsilon_y^0 + \epsilon_y^1 = v_{,y} + \frac{1}{2} w_{,y}^2 + w_{,y}w_{0,y} - \frac{w}{R} - zw_{,yy} \\ \gamma_{xy} &= \gamma_{xy}^0 + \gamma_{xy}^1 = u_{,y} + v_{,x} + w_{,x}w_{,y} + w_{0,x}w_{,y} + w_{,x}w_{0,y} - 2zw_{,xy} \end{aligned}\right\} (5)$$

STRESS-STRAIN RELATIONS

For stresses that do not exceed the elastic limit, Hooke's Law is valid; it is given by either

$$\left.\begin{aligned} \sigma_x &= E(\epsilon_x + \nu\epsilon_y)/(1-\nu^2) \\ \sigma_y &= E(\epsilon_y + \nu\epsilon_x)/(1-\nu^2) \\ \tau_{xy} &= E\gamma_{xy}/2(1+\nu) \end{aligned}\right\} (6)$$

or, in inverted form, by

$$\left.\begin{aligned} \epsilon_x &= (\sigma_x - \nu\sigma_y)/E \\ \epsilon_y &= (\sigma_y - \nu\sigma_x)/E \\ \gamma_{xy} &= 2(1+\nu)\tau_{xy}/E \end{aligned}\right\} (7)$$

POTENTIAL ENERGY

The total potential energy stored in the elastic shell under prescribed unit end shortening e (see Figure 1) is composed of the extensional and bending strain energies; it is given by

$$U = \frac{E}{2(1-\nu^2)} \int_{-L/2}^{L/2}\int_0^{2\pi R}\int_{-t/2}^{t/2}\left[(\epsilon_x+\epsilon_y)^2-2(1-\nu)\left(\epsilon_x\epsilon_y-\frac{\gamma_{xy}^2}{4}\right)\right] dxdydz \qquad (8)$$

Substitution of equations (5) in equation (8) and subsequent integration over the constant thickness t of the shell wall yields

$$U = \frac{Et}{2(1-\nu^2)} \int_{-L/2}^{L/2}\int_0^{2\pi R} \{(u_{,x}+\tfrac{1}{2}w_{,x}^2+w_{,x}w_{0,x}+v_{,y}+\tfrac{1}{2}w_{,y}^2+w_{,y}w_{0,y}-\tfrac{w}{R})^2$$

$$- 2(1-\nu)[(u_{,x}+\tfrac{1}{2}w_{,x}^2+w_{,x}w_{0,x})(v_{,y}+\tfrac{1}{2}w_{,y}^2+w_{,y}w_{0,y}-\tfrac{w}{R}) - \tfrac{1}{4}(u_{,y}+v_{,x}$$

$$+ w_{,x}w_{,y}+w_{0,x}w_{,y}+w_{,x}w_{0,y})^2]\}dxdy$$

$$+ \frac{D}{2}\int_{-L/2}^{L/2}\int_0^{2\pi R}[(w_{,xx}+w_{,yy})^2-2(1-\nu)(w_{,xx}w_{,yy}-w_{,xy}^2)]dxdy \qquad (9)$$

where $D = Et^3/12(1-\nu^2)$.

In accordance with the potential energy principle, U must have a stationary value with respect to admissible variation in the degrees of freedom u, v, and w in order for equilibrium to be achieved. As derived in Appendix I, the variation leads to the equilibrium equations

$$\left.\begin{aligned} N^0_{x,x} + N^0_{xy,y} &= 0 \\ N^0_{y,y} + N^0_{xy,x} &= 0 \\ D\nabla^4 w - \frac{N^0_y}{R} - N^0_x(w_{,xx}+w_{0,xx}) - N^0_y(w_{,yy}+w_{0,yy}) & \\ - 2N^0_{xy}(w_{,xy}+w_{0,xy}) &= 0 \end{aligned}\right\} \qquad (10)$$

and the accompanying boundary conditions at

$x = \pm \frac{L}{2}$:

$$\left.\begin{array}{ll}
\int_0^{2\pi R} N_x^0 dy = 0 & \text{or} \quad \delta u = 0 \\
\int_0^{2\pi R} N_{xy}^0 dy = 0 & \text{or} \quad \delta v = 0 \\
\int_0^{2\pi R} M_x dy = 0 & \text{or} \quad \delta w_{,x} = 0 \\
\int_0^{2\pi R} [N_x^0(w_{,x}+w_{0,x})+N_{xy}^0(w_{,y}+w_{0,y})+M_{x,x}+2M_{xy,y}]dy = 0 & \text{or} \quad \delta w = 0
\end{array}\right\} \quad (11)$$

$y = 0, 2\pi R$

$$\left.\begin{array}{ll}
\int_{-L/2}^{L/2} N_y^0 dx = 0 & \text{or} \quad \delta v = 0 \\
\int_{-L/2}^{L/2} N_{xy}^0 dx = 0 & \text{or} \quad \delta u = 0 \\
\int_{-L/2}^{L/2} M_y dx = 0 & \text{or} \quad \delta w_{,y} = 0 \\
\int_{-L/2}^{L/2} [N_y^0(w_{,y}+w_{0,y})+N_{xy}^0(w_{,x}+w_{0,x})+M_{y,y}+2M_{xy,x}]dx = 0 & \text{or} \quad \delta w = 0
\end{array}\right\} \quad (12)$$

$x = \pm \frac{L}{2}$, $y = 0, 2\pi R$:

$$M_{xy} = 0 \qquad \text{or} \quad \delta w = 0 \qquad (13)$$

ALTERNATE FORM OF TOTAL POTENTIAL ENERGY FUNCTIONAL

With the use of the middle surface strain-displacement equations (3), the total potential energy, equation (9), can be expressed in the form

$$U = \frac{Et}{2(1-\nu^2)} \int_{-L/2}^{L/2}\int_0^{2\pi R} [(\epsilon_x^0+\epsilon_y^0)^2-2(1-\nu)(\epsilon_x^0\epsilon_y^0-\frac{1}{4}\gamma_{xy}^{0^2})]dxdy$$

$$+ \frac{D}{2} \int_{-L/2}^{L/2}\int_0^{2\pi R} [(w,_{xx}+w,_{yy})^2-2(1-\nu)(w,_{xx}w,_{yy}-w,_{xy}^2)]dxdy \qquad (14)$$

Next, with the constitutive relations (7), written for the middle surface, the strains ϵ_x^0, ϵ_y^0, and γ_{xy}^0 can be replaced to give the total potential energy as

$$U = \frac{t}{2E} \int_{-L/2}^{L/2}\int_0^{2\pi R} [(\sigma_x^0+\sigma_y^0)^2-2(1+\nu)(\sigma_x^0\sigma_y^0-\tau_{xy}^{0^2})]dxdy$$

$$+ \frac{D}{2} \int_{-L/2}^{L/2}\int_0^{2\pi R} [(w,_{xx}+w,_{yy})^2-2(1-\nu)(w,_{xx}w,_{yy}-w,_{xy}^2)]dxdy \qquad (15)$$

The first two equilibrium equations (10) can be satisfied identically by the Airy stress function F, defined as

$$\left.\begin{aligned} N_x^0/t &= \sigma_x^0 = F,_{yy} \\ N_y^0/t &= \sigma_y^0 = F,_{xx} \\ N_{xy}^0/t &= \tau_{xy}^0 = -F,_{xy} \end{aligned}\right\} (16)$$

Finally, the introduction of the relationships between the middle-surface stresses σ_x^0, σ_y^0, and τ_{xy}^0 and the Airy stress function F defined by equations (16) permits the elimination of the stress components from equation (15); thus the desired alternate form of the total potential energy is

$$U = \frac{t}{2E} \int_{-L/2}^{L/2}\int_0^{2\pi R} [(F,_{yy}+F,_{xx})^2-2(1+\nu)(F,_{yy}F,_{xx}-F,_{xy}^2)]dxdy$$

$$+ \frac{D}{2} \int_{-L/2}^{L/2}\int_0^{2\pi R} [(w,_{xx}+w,_{yy})^2-2(1-\nu)(w,_{xx}w,_{yy}-w,_{xy}^2)]dxdy \qquad (17)$$

The total potential energy consists now of only two unknown quantities: the stress function F and the additional radial displacement w of the shell. With middle-surface equilibrium automatically satisfied through introduction of the stress function, the variational principle need be applied only with respect to w to achieve equilibrium out of the middle surface. However, it is necessary first to establish a relationship between F and w in order to present the total potential energy in terms of w alone. From displacement compatibility in the classical theory of elasticity, it is known that the middle surface displacements u and v must satisfy the condition

$$(u,_x),_{yy} + (v,_y),_{xx} - (u,_y+v,_x),_{xy} = 0 \tag{18}$$

With the strain-displacement equations (3) and the constitutive relations (7), written for the middle surface, the stress-displacement compatibility equation becomes

$$(\frac{\sigma_x^0}{E}),_{yy} + (\frac{\sigma_y^0}{E}),_{xx} - 2(\frac{\tau_{xy}^0}{E}),_{xy} = \nabla^2(\frac{\sigma_x^0+\sigma_y^0}{E}) = w,_{xy}^2 - w,_{xx}w,_{yy} - \frac{1}{R}w,_{xx}$$

$$+ 2w_0,_{xy}w,_{xy} - w_0,_{xx}w,_{yy} - w_0,_{yy}w,_{xx} \tag{19}$$

Then, by introducing the relations between the middle-surface stress components and the Airy stress function F of equations (16), the compatibility equation of von Kármán-Donnell shell theory is obtained for linear elastic behavior as

$$\nabla^4 F/E = w,_{xy}^2 - w,_{xx}w,_{yy} - \frac{1}{R}w,_{xx} + 2w_0,_{xy}w,_{xy}$$

$$- w_0,_{xx}w,_{yy} - w_0,_{yy}w,_{xx} \tag{20}$$

For any specific case, in order to eliminate the stress function F, the procedure is to solve equation (20) for F in terms of w. Then,

with F known, the total potential energy becomes a function of w alone. This procedure is not a simple one, since equation (20) lends itself to ready solution only when, for example, trigonometric series are used to express w. Further, it should be pointed out that the procedure is highly restricted in general to materials with constant elastic moduli (independent of the coordinates of the body) in view of the operations implicit in deriving equation (20) from equation (19).

METHOD OF SOLUTION

With the total potential energy applicable to both imperfect axially compressed curved plates and shells given by equation (17) in terms of the deflection w and the stress function F, the direct method of the calculus of variations (Rayleigh-Ritz method) is utilized to establish equilibrium-state, average stress-end shortening curves for various imperfection patterns.

CIRCULAR CYLINDRICAL SHELL

To study the various facets of the compressed circular cylindrical shell problem and to establish a better understanding of solutions obtained through von Kármán-Donnell theory, in conjunction with the potential energy method and trigonometric series to represent the radial displacement patterns, both initial and additional, several cases are investigated.

General Case of Present Analysis

A reasonable imperfection pattern for a long circular cylindrical shell is

$$\frac{w_0}{t} = A_{11}^0 \cos \frac{\pi x}{\lambda_{x_0}} \cos \frac{\pi y}{\lambda_{y_0}} + A_{20}^0 \cos \frac{2\pi x}{\lambda_{x_0}} \tag{21}$$

This expression represents a modification of the chessboard pattern into which a perfect cylinder buckles with infinitesimal amplitudes according to the classical theory (see references 1, 2, and 3). It is also both the experimentally observed buckle pattern of a compressed shell (see reference 18) and the modal pattern of a long thin cylinder undergoing free vibration with finite amplitudes (see reference 19). Thus, the initial pattern selected for w_0 is obviously one to which a compressed shell is particularly sensitive.

To provide for the growth of the initial pattern w_0 upon application of end shortening, the expression

$$\frac{w_0^*}{t} = A_{11}^* \cos\frac{\pi x}{\lambda_{x_0}} \cos\frac{\pi y}{\lambda_{y_0}} + A_{20}^* \cos\frac{2\pi x}{\lambda_{x_0}} \tag{22}$$

is assumed. Equation (22) ensures that the imperfection pattern w_0 retains its original wavelengths but is free to grow in amplitude through A_{11}^* and A_{20}^*.

The buckle mode for the shell is taken to be

$$\frac{w}{t} = A_{11} \cos\frac{\pi x}{\lambda_x} \cos\frac{\pi y}{\lambda_y} + A_{20} \cos\frac{2\pi x}{\lambda_x} + A_{02} \cos\frac{2\pi y}{\lambda_y} + A_{00} + \frac{w_0^*}{t} \tag{23}$$

It is to be noted that except for A_{00}, λ_{x_0}, and λ_{y_0}, all of the parameters in equation (23) are arbitrary; they are to be determined by application of the variational principle. That is, a stationary value of the total potential energy, equation (17), is sought with respect to A_{11}^*, A_{20}^*, A_{11}, A_{20}, A_{02}, λ_x, and λ_y. Since A_{00} actually vanishes before variation of the total potential energy, it is determined independently from enforcement of the periodicity condition governing the circumferential displacement v.

Of course, before the variation is carried out, equation (21) and equation (23) are substituted into equation (20) to determine F. Such a procedure leads to

$$\frac{F}{E} = -\frac{\sigma y^2}{2E} + \nabla^{-4}\left(w_{,xy}^2 - w_{,xx}w_{,yy} - \frac{w_{,xx}}{R} + 2w_{0,xy}w_{,xy} - w_{0,xx}w_{,yy} - w_{0,yy}w_{,xx}\right) \tag{24}$$

where σ has been introduced to provide for an average compressive stress acting on each shell cross section. The actual expression for F obtained by the operations indicated in equation (24) is illustrated in Appendix II. The average compressive stress is developed also in Appendix II for the same case and is shown to be

$$\frac{\sigma}{E} = e - \frac{t}{R}[\mu^2\eta(\frac{A_{11}^2}{8} + A_{20}^2) + \mu_0^2\eta_0(\frac{A_{11}^{*2}}{8} + A_{20}^{*2} + \frac{A_{11}^0 A_{11}^*}{4} + 2A_{20}^0 A_{20}^*)] \qquad (25)$$

where e is the prescribed unit end shortening and thus is the forcing function for the problem.

A typical average stress-unit end shortening curve for an assumed imperfection pattern wherein $A_{11}^0 = 1$, $A_{20}^0 = 0.25$, $\mu_0 = \lambda_{y_0}/\lambda_{x_0} = 0.52$, and $\eta_0 = \pi^2 Rt/\lambda_{y_0}^2 = 0.25$ is given in Figure 2. The values selected for μ_0 and η_0 correspond to the μ and η values of the stable portion of the Kempner[13] curve when $eR/t = 0.70$.

von Kármán-Tsien[8] Solution

The first solution of the von Kármán-Donnell theory for perfect shells appears in reference 8. The main contribution of this work lies in the qualitative rather than quantitative results, since the authors show the existence of equilibrium states with large as well as small (infinitesimal) displacements. The former imply that equilibrium stress states exist far below the one corresponding to classical buckling. This important finding became the plausible explanation for axially compressed thin cylinders in actual test to achieve only a small fraction of the classical buckling load.

The constrained deflection utilized by von Kármán and Tsien is equivalent to the deflection function of equation (23) with $w_0^* = 0$ and $A_{02} = A_{20}$. Typical von Kármán-Tsien average stress-end shortening curves are plotted in Figure 3 for $\mu = \lambda_y/\lambda_x = 1$ and several values of $\eta = \pi^2 Rt/\lambda_y^2$ (0.676, 0.400, 0.255, and 0.169). A curve obtained from the present analysis is plotted also in Figure 3 for $\mu = \lambda_y/\lambda_x = 1$, $A_{02} = A_{20}$, and η absolutely free.

Kempner[13] Solution

The first unconstrained solution of the von Kármán-Donnell theory for perfect axially compressed thin shells is given in reference 13. This solution, for the deflection function assumed (equation (23) with

$w_0^* = 0$ and A_{11}, A_{20}, A_{02}, μ, and η completely arbitrary) represents a true equilibrium solution, since all radial deflection parameters are permitted to vary in the application of the variational principle. The calculated points obtained by Kempner[13] to construct his average stress-end shortening curve are shown in Figure 4.*

Madsen-Hoff[12] Solution

In references 4 and 12, Hoff et al. point out the basic error of Donnell and Wan appearing in reference 11, that of actually permitting the imperfection pattern amplitude and wave shape to vary. In reference 12, the authors avoid the error by assuming an imperfection shape and permitting only the growth of the imperfection amplitude to vary. Their assumed initial imperfection shape and arbitrary buckle pattern are equivalent to equation (21) and equation (23) of the present work with $A_{11} = 0$, $A_{20} = 0$, and $A_{02} = 0$. The average stress-end shortening curves obtained on this basis are shown in Figure 5 for $A_{11}^0 = 0$, 0.1, and 0.17. Also shown in Figure 5 are the results of the present study for $A_{02} \neq 0$, $\lambda_y = \lambda_{y_0}$, $A_{11}^0 = 0.1$, and 0.17.

CIRCULARLY CURVED PLATE

Most of the research that has been conducted in connection with understanding the so-called "perplexing behavior" (see reference 5) of thin shells in compression has had, in reality, the goal of providing criteria for conventional shell structures used in aerospace design to withstand direct compression and bending loads. Such structures appear, in general, in stiffened rather than unstiffened form; hence, theoretical studies on pure monocoque shells under direct compression and bending loads have only limited value from the practical viewpoint.

A stiffened shell of the noncomposite type may be viewed as being made up of a series of curved plates separated by stringers and rings. Thus, it is of some importance to study the behavior of curved plates as

---

* Professor Joseph Kempner kindly provided the calculated points from which the continuous curve in reference 13 was plotted.

discrete structural elements and also to establish a knowledge of the transition from the well-understood behavior of flat plates to the not-so-well-understood behavior of complete cylinders as the curvature is gradually increased.

The shell theory presented in GENERAL THEORY and Appendix I is equally applicable to curved and flat $(R \to \infty)$ plates simply by changing the limits of integration in the circumferential direction in the potential energy expression (equation (17)) and the boundary conditions (equations (11)-(13)) from $y = 0, 2\pi R$ to $y = -\frac{b}{2}, \frac{b}{2}$. Naturally, the same changes would occur in the developments of Appendix I. A long curved plate element is shown in Figure 1, along with the sign convention used in the analysis.

For a first approximation to the behavior of a circularly curved plate under prescribed end shortening, the radial deflection function is taken as

$$\frac{w}{t} = A_{11} \cos \frac{\pi x}{\lambda_x} \cos \frac{\pi y}{\lambda_y} + A_{01} \cos \frac{\pi y}{b}, \qquad \frac{b}{\lambda_y} = 1,3,5\ldots \tag{26}$$

The first term is sufficient to establish quite accurately the average stress-end shortening curve for a long rectangular flat plate $(R \to \infty)$ with pinned edges until the end shortening exceeds the critical end shortening by an order of magnitude (see reference 20). For shallow-curved plates $(Z = b^2/Rt \leq 10)$, the second term in equation (26) is sufficient to provide reasonably accurate average stress-end shortening curves dependent upon Z. Through the use of equation (26) and the total potential energy given by equation (17) (with suitable integration limits for the circumferential direction), application of the variational principle leads to the average stress-end shortening curves plotted in Figure 6, when $\mu = \lambda_y/\lambda_x = 1$, $N = b/\lambda_y = 1$, and $Z = 10$ and 20, respectively. Also, in Figure 6, are shown corresponding results for an improved approximation to the radial deflection function; that is,

$$\frac{w}{t} = A_{11} \cos \frac{\pi x}{\lambda_x} \cos \frac{\pi y}{\lambda_y} + A_{01} \cos \frac{\pi y}{b} + A_{21} \cos \frac{2\pi x}{\lambda_x} \cos \frac{\pi y}{\lambda_y} \qquad (27)$$

The details of the curved plate analysis are given in Appendix III. It is to be noted that the behavior of a shallow curved plate ($Z \leq 10$) is similar to that of a flat plate; thus, the curved plate is relatively insensitive to initial deviations (see reference 21).

RESULTS AND DISCUSSION

CIRCULAR CYLINDRICAL SHELL

An investigation of the bending, buckling, and postbuckling of initially imperfect circular cylindrical shells under axial compression has been undertaken to establish a clearer understanding of the many solutions obtained through the use of von Kármán-Donnell shell theory, the potential energy method, and trigonometric series to represent the radial displacement patterns.

General Case of Present Analysis

The most general solution of the present study is based upon the assumed initial and additional radial displacement functions given by equations (21) and (23). The assumed waveform differs from that of Kempner only in the stipulation of an imperfection pattern and the allowance for its growth in amplitude. With w_0 and w_0^* set equal to zero, the stable branch of the average stress-end shortening curve first obtained by Kempner with 5 free parameters is duplicated in Figure 2 by the lower curve. The upper curve represents a 7-free-parameter solution obtained from the present analysis with $A_{11}^0 = 1$, $A_{20}^0 = 0.25$, $\mu_0 = \lambda_{y_0}/\lambda_{x_0} = 0.52$, and $\eta_0 = \pi^2 Rt/\lambda_{y_0}^2 = 0.25$. The values of μ_0 and η_0 correspond to those of Kempner when $eR/t = 0.70$. The curve is of interest because it shows that unlike average stress-end shortening curves for postbuckled shells as presented by, for example, Donnell and Wan,[11] Loo,[22] and Madsen and Hoff,[12] any perfect body solution is a lower rather than upper bound to the imperfect body behavior when the von Kármán-Donnell theory is utilized in combination with trigonometric series and the Rayleigh-Ritz procedure. A more meaningful interpretation of the two curves in Figure 2 is presented later in connection with the detailed discussion of the Kempner[13] solution as reevaluated in the present analysis.

von Kármán-Tsien Solution

Although the von Kármán-Tsien solution was undertaken in a qualitative fashion only, mainly to offer a plausible explanation for the failure of

compressed shells in experiments to reach more than a small fraction of the classical buckling load, many subsequent investigators have attributed quantitative results to von Kármán-Tsien which the authors themselves never claimed.

Thus, as a first step in evaluating the existing work on the postbuckling behavior of imperfect shells, the von Kármán-Tsien solution was reviewed in the light of the present analysis approach. On the basis of equation (23), with $w_0^* = 0$ and $A_{02} = A_{20}$, the curves plotted in Figure 3 were obtained. The solid curves in the postbuckling region represent identically the results obtained by von Kármán and Tsien for $\mu = 1$ and the designated values of η. The dashed curve is the result of the present analysis when $\mu = 1$ and η is a free variable. Of importance is the fact that for $\mu = 1$, the lowest postbuckling stress on a minimum potential energy basis is given by $\sigma R/Et = 0.245$. The lowest postbuckling stress obtained by von Kármán and Tsien appears on the $\eta = 0.255$ curve and is given by $\sigma R/Et = 0.194$. Leggett and Jones[9] noted, with respect to the results of von Kármán and Tsien, that the lowest postbuckling stress obtained for a fixed μ and discrete values of η is not necessarily that corresponding to a minimum energy at the fixed value of μ. This can be illustrated in Figure 3 by noting that only certain points on each η-curve correspond to points on the true minimum energy curve for the deflection assumed and $\mu = 1$. The important fact is that the minimum stress obtained from the envelope of the discrete η-value curves is lower than the postbuckling stress corresponding to the minimum-energy solution for the fixed value of μ. In other words, in systems which possess unstable branches of the postbuckling curves, it is not permissible to obtain the lowest stress by minimizing the load with respect to the buckling parameters. It is interesting, nevertheless, that with the same deflection function

$$\frac{w}{t} = A_{11} \cos \frac{\pi x}{\lambda_x} \cos \frac{\pi y}{\lambda_y} + A_{20} \cos \frac{2\pi x}{\lambda_x} + A_{02} \cos \frac{2\pi y}{\lambda_y} + A_{00},$$

and $A_{20} = A_{02}$, the von Kármán-Tsien minimum postbuckling stress of

$\sigma R/Et = 0.194$ (obtained for $\mu = 1$ and $\eta = 0.255$) compares almost identically with the minimum postbuckling stress, $\sigma R/Et = 0.195$, obtained by Leggett and Jones[9] and Michielsen[10] on the basis of free variation with respect to both μ and η.

Kempner Solution

Although a portion of the stable branch average stress-end shortening curve of the Kempner solution has been shown in Figure 2, the solid-curve result presented by Kempner in reference 13 is shown in Figure 4 in terms of the actual calculated points (see footnote on page 14). The solid curve of Figure 4 is the result obtained in the present analysis with the aid of a high-speed computer. The desk-calculator results obtained by Kempner in a remarkable effort are quite accurate along the stable branch of the average stress-end shortening curve. However, even though the remaining points appear to indicate that the postbuckling curve closes to the bifurcation point, the very accurate numerical results of the present analysis show that (1) the left-hand portion of the lower branch of the solution cannot be extended economically for $\sigma R/Et > 0.334$, a Burroughs B-5500 computer notwithstanding, and (2) another solution of completely unstable character exists for $\sigma R/Et > 0.387$.

The loop appearing below the bifurcation point is not a new result. Thielemann, in Figure 10 of reference 23, notes that Donnell's solution yields the same phenomenon. However, in the Donnell and War[11] study referred to by Thielemann, the authors mention only that success was achieved in finding a solution emanating from the bifurcation point downward to $\sigma R/Et = 0.45$. The unstable solution moving upward from the bifurcation point is considered a new result in view of its absence from the literature.

Another new result of the present analysis, incidentally, is the average stress-end shortening curve shown in Figure 7. This solution corresponds to the deflection function, equation (23), with $w_0^* = 0$, $A_{02} = 0$, and a free variation of the total potential energy with respect to

A_{11}, A_{20}, μ, and η. The curve of Figure 7 is not much different from that of Kempner in Figure 4. The minimum equilibrium postbuckling stress parameter is given by $\sigma R/Et = 0.195$. This minimum value is significant in that it has been obtained on the basis of a buckle pattern which is a first modification of the classical-theory chessboard pattern. From the discussions contained in the studies presented by von Kármán-Tsien,[8] Leggett and Jones,[9] Michielsen,[10] and Kempner,[13] the implication is always present that the low minimum postbuckling stresses obtained are associated with the "diamond" buckle pattern developed by von Kármán and Tsien on the basis of physical observation which automatically includes the A_{02} term in equation (23).

The difficulty in obtaining an economically feasible solution beyond $\sigma R/Et = 0.334$ (on the unstable portion of the curve) is attributed to the fact that, for small increments in the applied unit end shortening (see Figure 4), the buckle maximum amplitude, nondimensionalized with respect to the wall thickness t, is growing very rapidly whereas μ and η are becoming quite small in magnitude. The buckle pattern free coefficients A_{11}, A_{20}, and A_{02} are given in Figure 8 as functions of eR/t; the free parameters μ and η are given in similar fashion in Figure 9.

The tedious and, hence, cost-consuming computations necessary to seek a converged solution of the five nonlinear equations in A_{11}, A_{20}, A_{02}, μ, and η are not justified because the portion of the average stress-end shortening curve in question represents application of the von Kármán-Donnell theory in a range where it is no longer valid for practical considerations; the limitation on either the size of the rotations or the linear-elastic constitutive law is being exceeded, and the results have meaning only for shells of extremely high R/t ratios. The limitations of von Kármán-Donnell theory with respect to permissible rotations and onset of inelastic deformations for axially compressed perfect shells in the R/t range of practical interest have been pointed out by Mayers and Rehfield.[16] In fact, in reference 16 it is shown that the Kempner solution of reference 13 based on von Kármán-Donnell theory

is the lower bound to a family of R/t-dependent average stress-end shortening curves and corresponds to the case of $R/t \to \infty$.

The present-analysis solution shown in Figure 4 for $\sigma R/Et > 0.387$ does not exceed the kinematic limitations on von Kármán-Donnell theory, as the maximum deflections are of the order of the wall thickness; however, it is of no practical value because it represents unstable equilibrium. Above the bifurcation point, however, it is of interest to note that the thin-shell theory is attempting to produce thick-shell behavior (axisymmetric buckling) because, as indicated in Figure 9, $\eta \to 0$ and $\mu \to \infty$.

The von Kármán-Donnell theory, Kempner-type, axially compressed perfect shell solution with more terms included in the radial deflection function w (equation (23) with $w_0^* = 0$) has been given by Almroth[14] (nine free parameters) and Hoff et al.[15] (15 free parameters). Although Almroth succeeded in obtaining a minimum postbuckling equilibrium stress corresponding to $\sigma R/Et = 0.0652$, Hoff et al. succeeded in lowering the minimum postbuckling stress parameter $\sigma R/Et$ to 0.0427. From the overall results of reference 15, the authors are able to conclude that when the radial deflection is represented by an infinite series, the completely free parameter solution of the von Kármán-Donnell theory for the axially compressed perfect shell is represented by $w \to 0$, $\mu \to 0$, $\eta \to 0$, and a minimum postbuckling equilibrium stress parameter $\sigma R/Et \to 0$. The buckle shape itself approaches a perfect Yoshimura[17] developable surface (vanishing membrane strain). Thus, on the basis of the findings reported in references 15 and 16, it took from 1941 to 1965 to establish that the rigorous stable solution of the von Kármán-Donnell theory for an axially compressed perfect shell with (1) a finite number of assumed buckle-pattern parameters absolutely free applies only to an infinitely thin shell ($R/t \to \infty$) and with (2) an infinite number of assumed buckle-pattern parameters which are absolutely free leads to the trivial solution that the infinitely thin shell buckles at a vanishingly small stress.

Some final remarks are in order relative to the present-analysis solution shown in Figure 2 and that of Kempner shown in both Figures 2 and 4. Obviously, with decreasing initial-imperfection amplitudes, the present-analysis curve of Figure 2 coalesces into the lower branch of the Kempner curve. Now, when the initial deviation pattern wavelengths are larger than the wavelengths occurring in the Kempner solution, an increase of the initial-imperfection amplitudes will not affect the Kempner solution because the Kempner buckle shape is physically able to govern the behavior. On the other hand, when the initial-deviation-pattern wavelengths are smaller than the wavelengths occurring in the Kempner solution, the initial-deviation pattern governs and grows in amplitude; the Kempner buckle pattern is constrained from occurring, which means that an increase in the potential energy occurs. Thus, the minimum postbuckling stress of the imperfect shell is greater than the minimum postbuckling stress obtained from the Kempner solution. The implication, then, is that stiffening elements could be placed on a thin shell with spacing so arranged that the snap-through buckle pattern cannot occur. This behavior has been illustrated in the laboratory by buckling two identical cylinders which were commercially fabricated on an automated assembly line. One cylinder is buckled in the unstiffened configuration so as to discern the buckle pattern. The remaining cylinder is tested with very light stiffeners located so as to hinder the original buckle pattern from forming. A significant increase in buckling load (almost 50 percent) has resulted with a very small weight penalty. Photographs of the two specimens tested to substantiate this behavior are shown in Figure 10. The remarkable decrease in buckle amplitude of the lightly stiffened cylinder should be noted. The buckle pattern of the unstiffened cylinder is of interest because of its similarity to the Yoshimura[17] buckle pattern. The latter is a polyhedral surface of plane triangles developable from the middle surface of a circular cylindrical shell. Conventional cylinders tested in the laboratory tend toward Yoshimura-type buckles only in localized bands. The preformed plastic hinges shown in the test cylinder of Figure 10 provide the mechanism for the development of the Yoshimura buckle pattern over almost the entire surface of the unstiffened specimen.

Madsen-Hoff Solution

The behavior of postbuckled, axially compressed, perfect circular cylindrical shells leading to the trivial solution (for an infinite number of terms in the trigonometric series representing the radial deflection function) discussed in the preceding section has been explained by Madsen and Hoff.[12] The authors of reference 12 point out that a variation of the total potential energy with respect to all buckle-pattern parameters is unrealistic in view of the fact that a cylinder of finite R/t ratio cannot buckle into less than 2 circumferential full waves. Thus, in reality, the trivial solution cannot occur.

In the same reference, Madsen and Hoff then proceed to investigate the behavior of practical shells in order to estimate the magnitude of the maximum stress reached in the presence of imperfections. Although the behavior of imperfect shells in axial compression had been investigated by Donnell and Wan,[11] Madsen and Hoff discerned an error in the Donnell-Wan procedure and thus justified further investigation of the problem. Fundamentally, the criticism of the Donnell-Wan procedure, as noted by Madsen and Hoff, is that the total potential energy should not be minimized with respect to any of the parameters describing the initial deviation shape. Some of the results of their analysis based on the correct procedure are given in Figure 5 for a specified imperfection pattern. The deflected shape is obtainable from equations (21) and (23) of the present analysis when $A_{11} = 0$, $A_{20} = 0$, and $A_{02} = 0$. The curve of Figure 5 for $A_{11}^0 = 0$ is based upon a fixed μ_0 and η_0. The postbuckling curve for A_{11}, A_{20}, μ, and η as free variables, as discussed earlier, has been obtained for the first time in the present analysis (see Figure 7). The significance of $\mu_0 = 1.0$ and $\eta_0 = 0.826$ is related to the only reasonable physical solution of the linearized problem solved by Madsen and Hoff. It is of interest to note, however, that Loo,[22] by making the arbitrary assumption that $\mu = 1$, was able to calculate that $\eta = 0.826$ at the bifurcation point. Of further interest is the fact that the present analysis leads to the values $\mu = 1$ and $\eta = 0.826$ in a free variation of the nonlinear formulation at the

bifurcation point; in addition, it can be seen from Figure 9 that, on the basis of extrapolation, another set of μ and η values (approximately, $\mu = 0.345$ and $\eta = 0.320$) exists at the bifurcation point.

The imperfect shell average stress-end shortening obtained by Madsen and Hoff for $A_{11}^{0} = 0.1$ is given in Figure 5 as a solid curve. A distinct maximum stress is evidenced. This maximum, the conclusions of reference 12 notwithstanding, is not the lowest maximum stress to be expected. The addition of the A_{02} term in equation (23) leads to the dashed curve in Figure 5 on the basis of the present analysis when $\lambda_y = \lambda_{y_0}$. In addition, for the case when $A_{11}^{0} = 0.17$, the inclusion of the A_{02} term removes the concept of an initial maximum stress. Thus, it is evident that maximum stress calculations for reasonably imperfect shells based on the Madsen-Hoff procedure should include sufficient terms in the assumed deflection function to guarantee a converged solution. This means that the maximum stress is sensitive not only to the amplitude of the initial deviation but also to the waveform of the buckle pattern. Finally, it is important to note that maximum stress calculations should not overlook the possibility of yielding of the material. A maximum strength analysis of axially compressed imperfect shells, including inelastic deformation, has been presented by Mayers and Wesenberg,[24] in which a modified version of Reissner's variational principle is utilized.

CIRCULARLY CURVED PLATE

The analysis of the long curved plate undertaken in this investigation is important from the standpoint that conventional aerospace vehicle shell structures are generally of the semimonocoque rather than pure-monocoque type. That is, the pure monocoque thin shell discussed in the previous section is stiffened by stringers and rings in actual practice in order to overcome the tendency of pure-monocoque thin shells to buckle at stresses well below the classical value under direct compression and bending loads. To date, despite extensive theoretical and experimental studies, the optimum semimonocoque shell for a given loading (that is, the sizing of stiffeners and shell thickness and the spacing of stiffeners) cannot be designed on the basis of theoretical analysis

alone. It is unusual that so much attention and effort has been devoted to pure-monocoque shells when the fundamental structural component existing between stringers and rings of semimonocoque shells (the actual case) is a curved plate. This is certainly true when discrete stiffening is utilized and conceptually true in the case when analysts consider that sufficiently closely spaced stiffeners and rings may be "smeared out" over the shell surface. However, even in the latter case, information is necessary to establish geometrical properties (including spacing of the stiffeners), supposedly to preclude the occurrence of local buckling between stiffening elements.

The average stress-end shortening curves appearing in Figure 6 for $Z = 10$ and 20, respectively, based upon the radial deflection function of equation (26) and the variational development of Appendix III (with $\mu = 1$ and $\lambda_y = b$), are considered to be extremely significant. It is to be noted that when the plate is flat $(R \to \infty, Z \to 0)$, the well-known behavior reflects the ability of the plate to carry additional load beyond the bifurcation point. As shown in reference 25, this behavior is limited only by the phenomena of eventual buckle pattern change and the onset of inelastic deformations. Under the assumption of elastic behavior in the present analysis, the solid-curve result in Figure 6 for a shallow-curved plate $(Z = 10)$ suggests that catastrophic snap-through buckling can be avoided and a load-carrying ability in the vicinity of the classical value can be maintained. With $Z = 20$, the snap-through does occur, but it cannot be considered catastrophic from the load-carrying-ability standpoint. Even when the improved radial deflection function (equation 27) is introduced, only about a ten percent reduction in load-carrying ability is evidenced. However, for $Z = 40$ and 60, the present analysis computations indicate that thin-cylinder behavior (catastrophic snap-through) governs. The lower bound to such behavior for the present analysis (with $A_{21} = 0$) is given by the lowermost solid curve. This curve is the same as that appearing in Figure 5 for a perfect cylinder which buckles and postbuckles with $\mu = 1$ and $\eta = 0.826$.

The primary question, of course, concerns the weight penalty involved in sizing stiffened shells such that the panel behavior between stiffeners and rings is given by results similar to those plotted in Figure 6. Apparently, in practice, cylinders with stiffeners spaced sufficiently close together that the "smearing out" concept may be used are specifically designed such that local buckling of the sheet material between stiffeners is prevented. For example, the recent preliminary design procedure presented by Smith and Spier[26] for stringers and/or ring-stiffened circular cylinders under axial compression commences with the fundamental step that precludes buckling of the curved sheet lying between the stiffening elements of the overall cylinder. As another example, the recent shell analysis manual prepared by Baker et al.[27] recommends (1) the design formula

$$\sigma_{cr} = \eta C \frac{\pi^2 E}{12(1-\nu^2)} \left(\frac{t}{b}\right)^2 , \qquad Z < 30 \qquad (28)$$

to determine the buckling stress for the curved plate elements between stringers and rings and (2) the generous knock-down values for C extending from 40 percent for $R/t = 100$ to 55 percent for $R/t = 500$, the practical R/t-ratio range for the sheet material in stiffened cylinders. The coefficient η in equation (28) has been introduced in reference 27 as a correction factor when inelastic buckling occurs.

To study the implications of the present results (see Figure 6) as they might apply to achieving increased efficiency of axially compressed stiffened shells, a particular cylinder tested by Card and Jones[28] has been selected. The cylinder geometry and elastic constants are given in Figure 11. It is noteworthy that even though the effective R/t ratio of the "smeared out" cylinder is 167, the "effectively" thick cylinder buckled in a typical thin-cylinder "diamond" configuration (see Figure 3b of reference 28). This would tend to indicate a significant sensitivity to initial deviations from a uniform circular shape.

For the cylinder section of Figure 11, the Z of the curved plate between 60 stringers spaced 1.0 inch apart is 3.74. Now, when every other

stringer of the 60 stringers is removed, Z becomes 14.96. In an attempt to provide for the formation of nodes at each remaining stringer, the criterion given by Schildcrout and Stein[29] for axially compressed curved plates with simply supported edges has been used with the result that the depth of the stringers must be increased to $t_s = 0.336$ inch The increased stringer material is "borrowed" from the 30 stringers that have been removed. Next, the remaining material from the removed stringers is distributed as 20 rings of the same geometry as the 30 redesigned stringers. With curved square sections, the criterion given by Batdorf and Schildcrout[30] for simply supported compressed curved rectangular plates with central chordwise stiffeners implies that nodes should form at each shell ring independent of the stiffness of the ring cross section. The ring spacing has been selected to give $\mu = 1$ in every curved-plate element. From Figure 6, it can be seen that the average stress remains in the vicinity of the classical stress for $Z = 14.96$. Thus, for a 6 percent increase in weight of the entire cylinder, the classical load obtained from the buckling criterion given by Block et al.[31] is 6.55 times greater than the corresponding buckling load for the original cylinder with 60 longitudinal stringers and no rings. Even though the quantitative results may not be practically useful, the qualitative trend cannot be overlooked. That is, a judicious redesign with respect to the rings should both lighten the cylinder and reduce the buckling load to a practical level. The attempt should be made to determine, by iteration, the lightest cylinder for $Z < 20$ and an effective radius-to-thickness ratio below about 250. For example, a trade-off study could be undertaken with respect to the effects of (1) lightening the 20 rings and (2) doubling the spacing between the existing rings and, if necessary, increasing the ring stiffness through use of the material available from the removed rings. In any event, the impressive results obtained herein with respect to the potential increase in efficiency of the cylinder tested by Card and Jones[28] cannot be disregarded. For eccentrically stiffened cylinders, the decrease in effective radius-to-thickness ratio minimizes the sensitivity to initial

imperfections. The appearance of "diamond" buckles in the cylinder test, even with the effective R/t ratio equal to 167, suggests that ring stiffening can only aid in alleviating the imperfection sensitivity. Finally, the sample calculations show that rings can be added at little or no increase in weight by redesigning the stringers with respect to section properties and spacing.

CONCLUDING REMARKS

The extensive study presented has made it possible to understand to a greater degree the long-standing and enigmatic behavior of thin circular cylindrical shells in axial compression. The significant contributions of Donnell,[7] von Kármán and Tsien,[8] and Kempner[13] stemming from their investigations of perfect elastic shells have been reevaluated on the basis of the present analysis and some new results and interpretations given the earlier works. With regard to the behavior of imperfect shells, the analyses of Donnell and Wan[11] and Madsen and Hoff[12] have been studied, also, and the results of the latter authors have been extended.

On the basis of the understanding of pure-monocoque shell behavior, an investigation of the postbuckling behavior of curved plates has led to significant results concerning the transition region from flat plates to highly curved plates and complete cylinders. The curved plate behavior is significant in that the conventional thin shell utilized in aerospace structures design is of the semimonocoque (stiffened) rather than the pure-monocoque configuration. Thus, the basic structural shell elements are the curved plates existing between stringers and rings. In the absence of any known theoretical analysis which can predict the maximum load in axial compression of a given stiffened shell, the present investigation offers some new concepts which appear to justify the preliminary design of optimized conventionally (stringer-ring) stiffened shells on the basis of nonlinear curved plate analysis in conjunction with stringer-ring sizing and spacing based upon (1) the postbuckling results obtained herein for unstiffened thin shells and (2) the linear-theory results of Schildcrout and Stein[29] and Batdorf and Schildcrout[30] for axially compressed, simply supported, curved plates with axial and chordwise central stiffeners, respectively. The qualitative results obtained relative to achieving buckling loads of stiffened cylinders in the vicinity of the classical value cannot be overlooked. Further research in this area is mandatory because of the desperate requirement for weight reduction in aerospace structures. The latest design manuals (1967-68)[26,27,32,33] still contain cautionary remarks to the effect, for

example, that "A currently popular viewpoint is to consider classical theory to be directly applicable to most practical stiffened shells. Nevertheless, to account for uncertainties and to guard against reckless extrapolation into extreme parameter ranges, it is suggested here that a knock-down factor be retained in the buckling analysis of stiffened cylinders. This should result in conservative strength estimates which can be employed with confidence in the design of actual hardware." Unfortunately, the knock-down factors suggested are very little different from those which have been generously utilized in practice for the past 25 years at the expense of overweight and uneconomical designs. If optimized design criteria are not available for conventional shell construction, then what hope is there that such criteria will soon be available for shells in which promising composites are to be employed (for example, sandwich, laminated, and fiber-reinforced materials)?

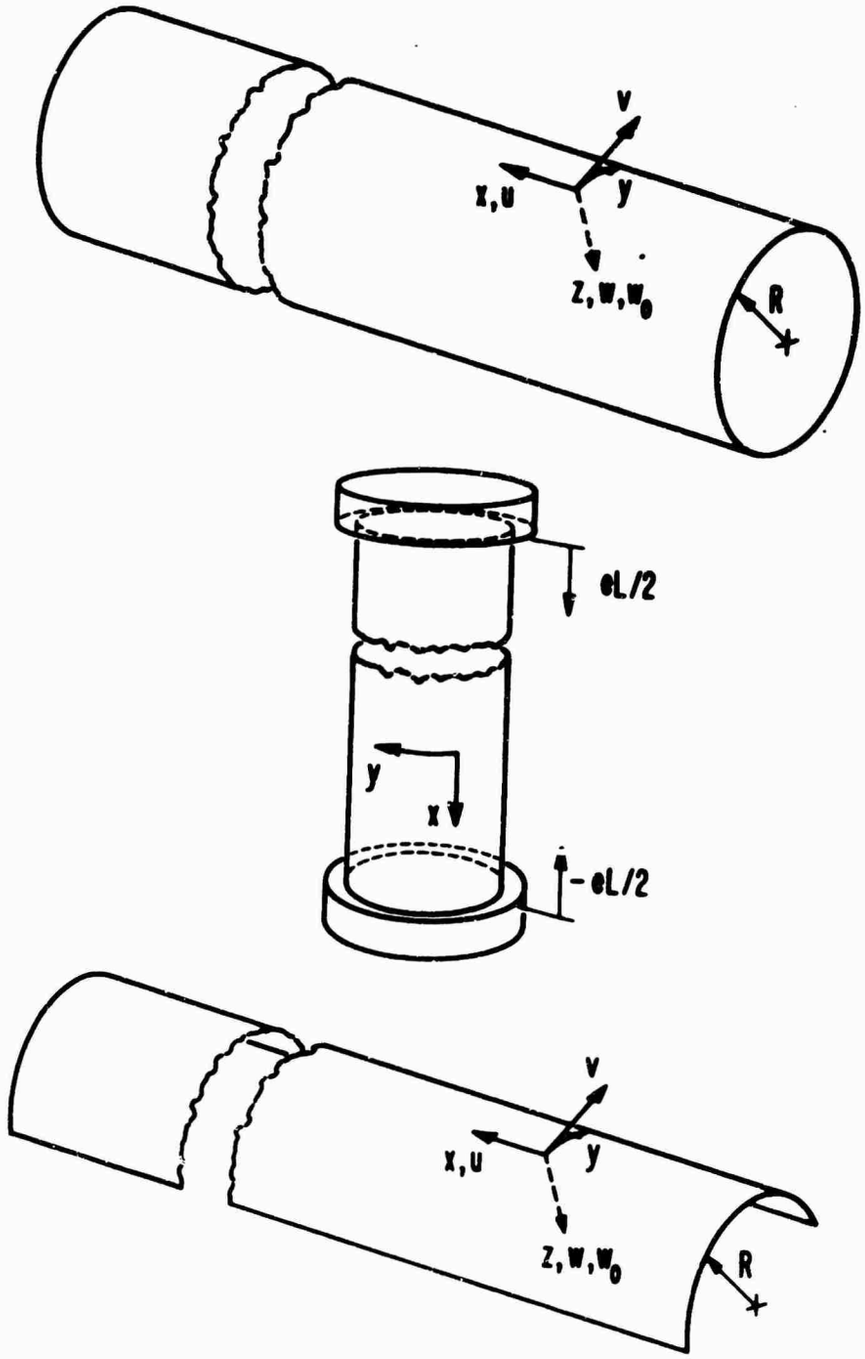

Figure 1. Geometry and Sign Convention for Curved Plate and Complete Shell.

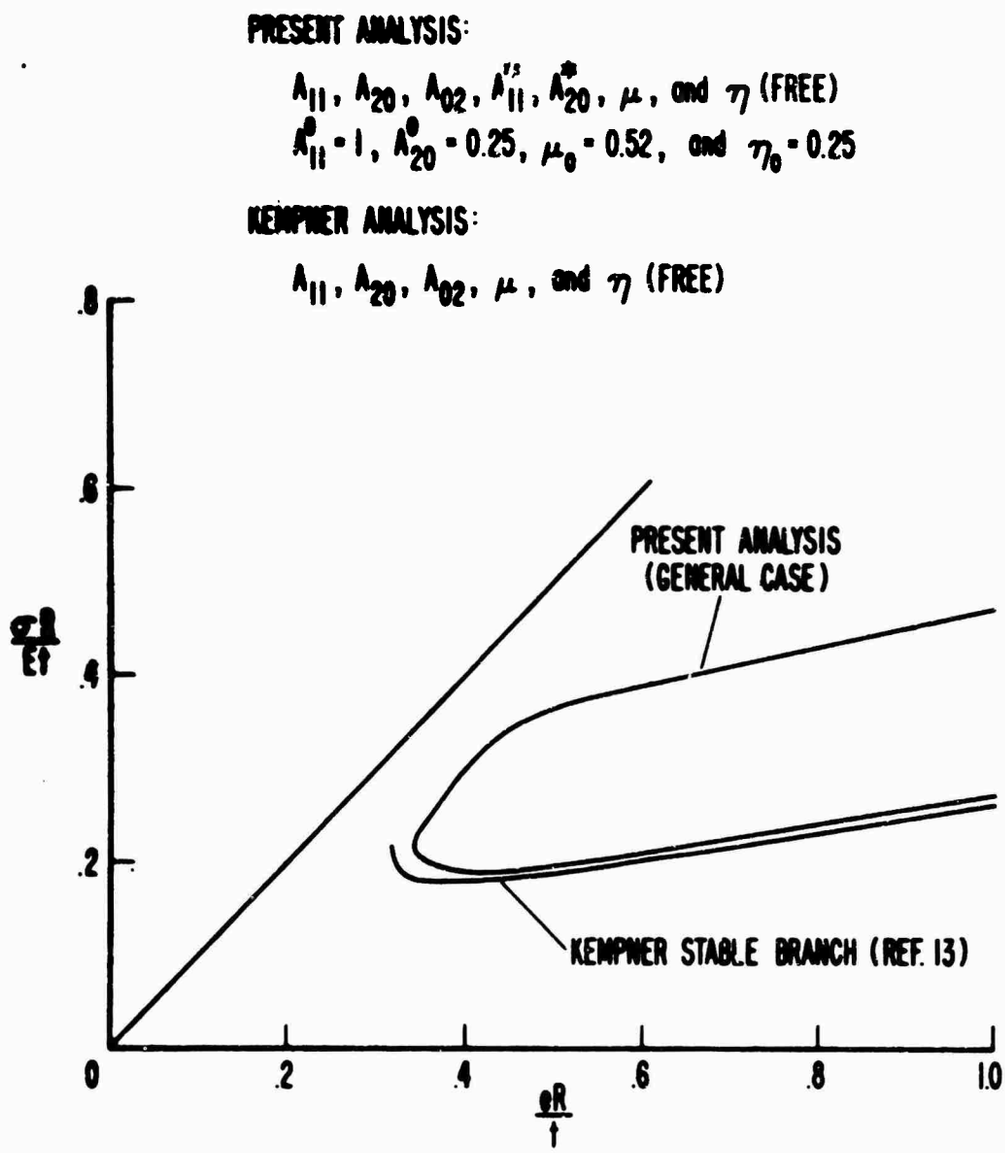

Figure 2. Average Stress-Unit End Shortening Curves (Present Analysis and Reference 13).

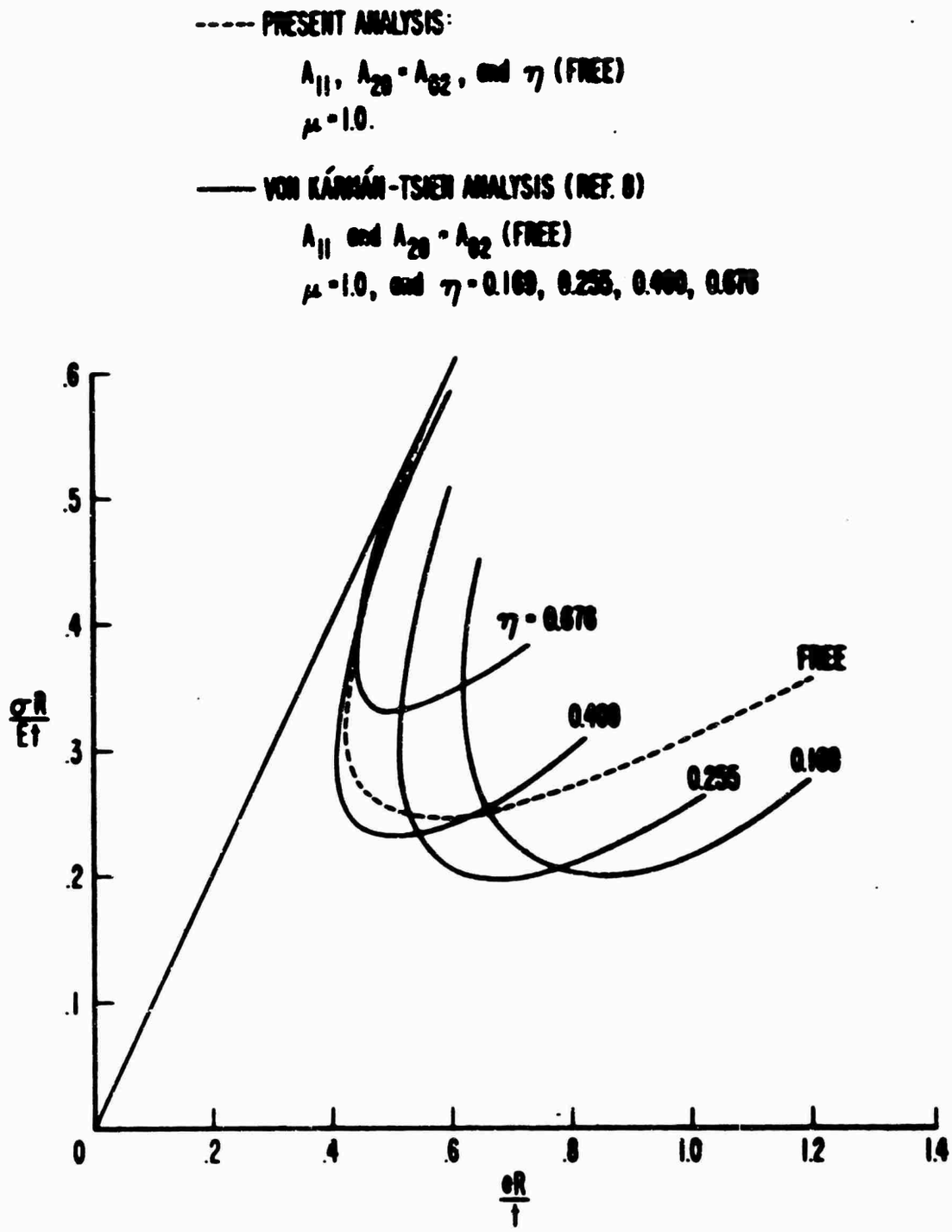

Figure 3. Average Stress-Unit End Shortening Curves (Present Analysis and Reference 8).

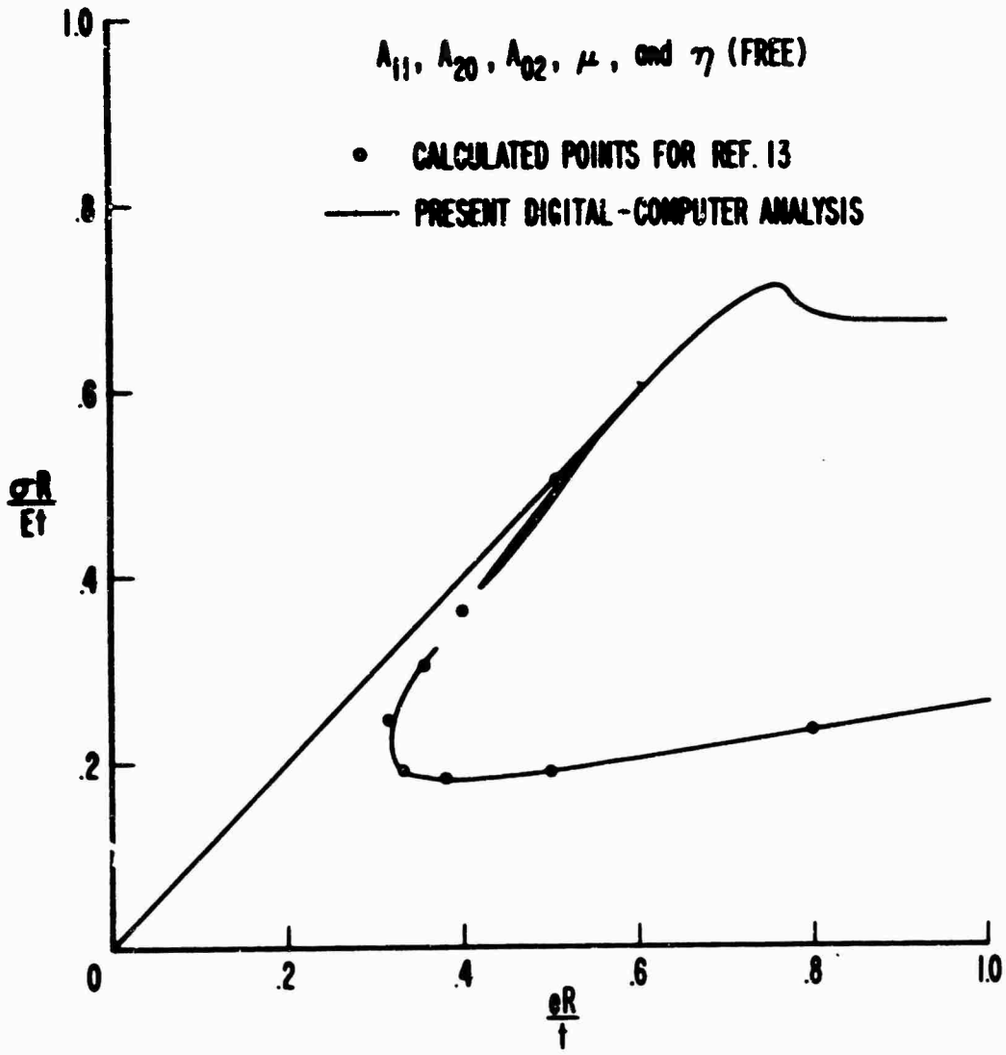

Figure 4. Average Stress-Unit End Shortening Curve for Kempner Radial Deflection Function (Present Analysis Digital Computer Solution and Desk Calculator Points Obtained in Reference 13).

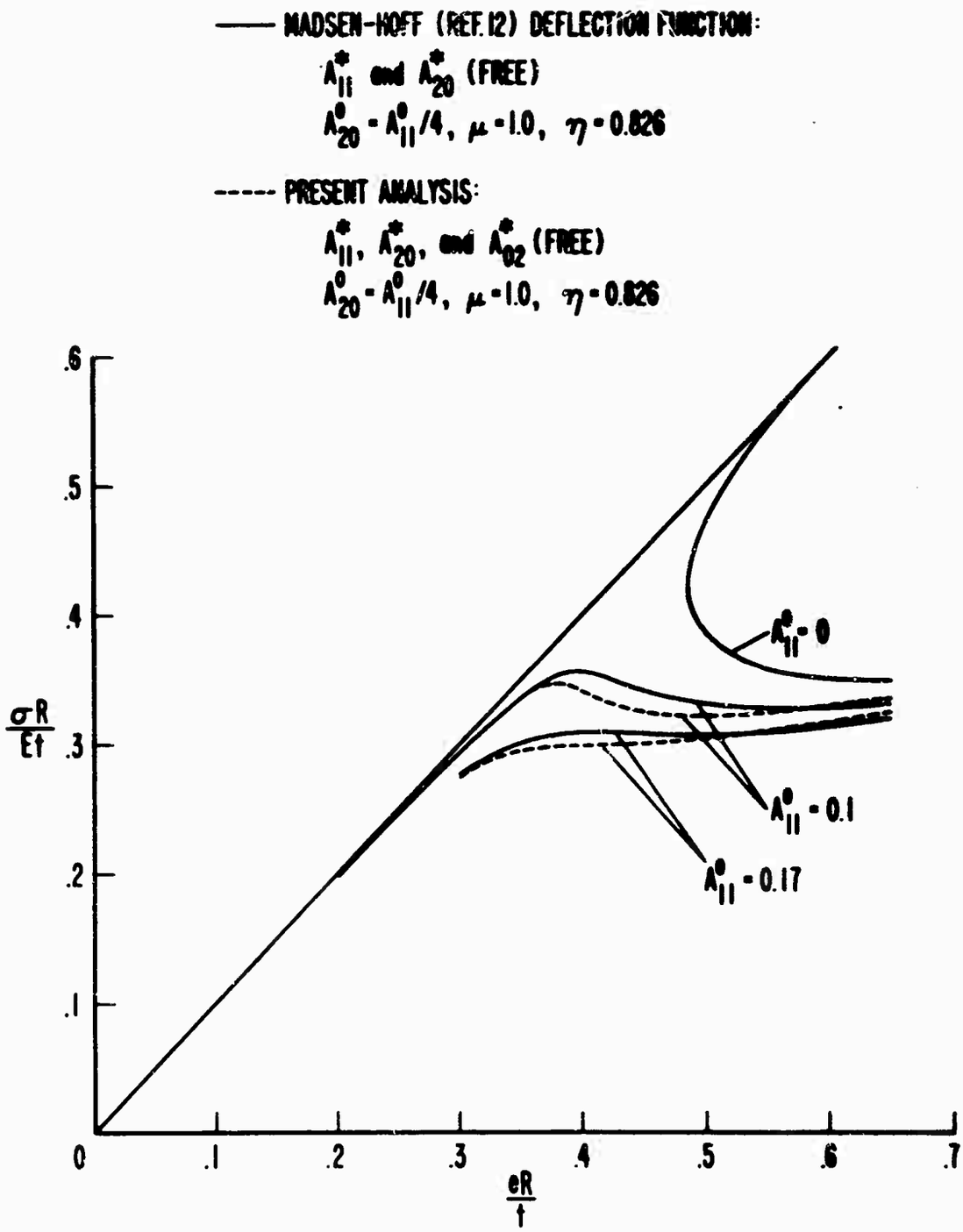

Figure 5. Average Stress-Unit End Shortening Curves for Perfect and Imperfect Shells (Comparison of Present Analysis Solutions With Those of Reference 12).

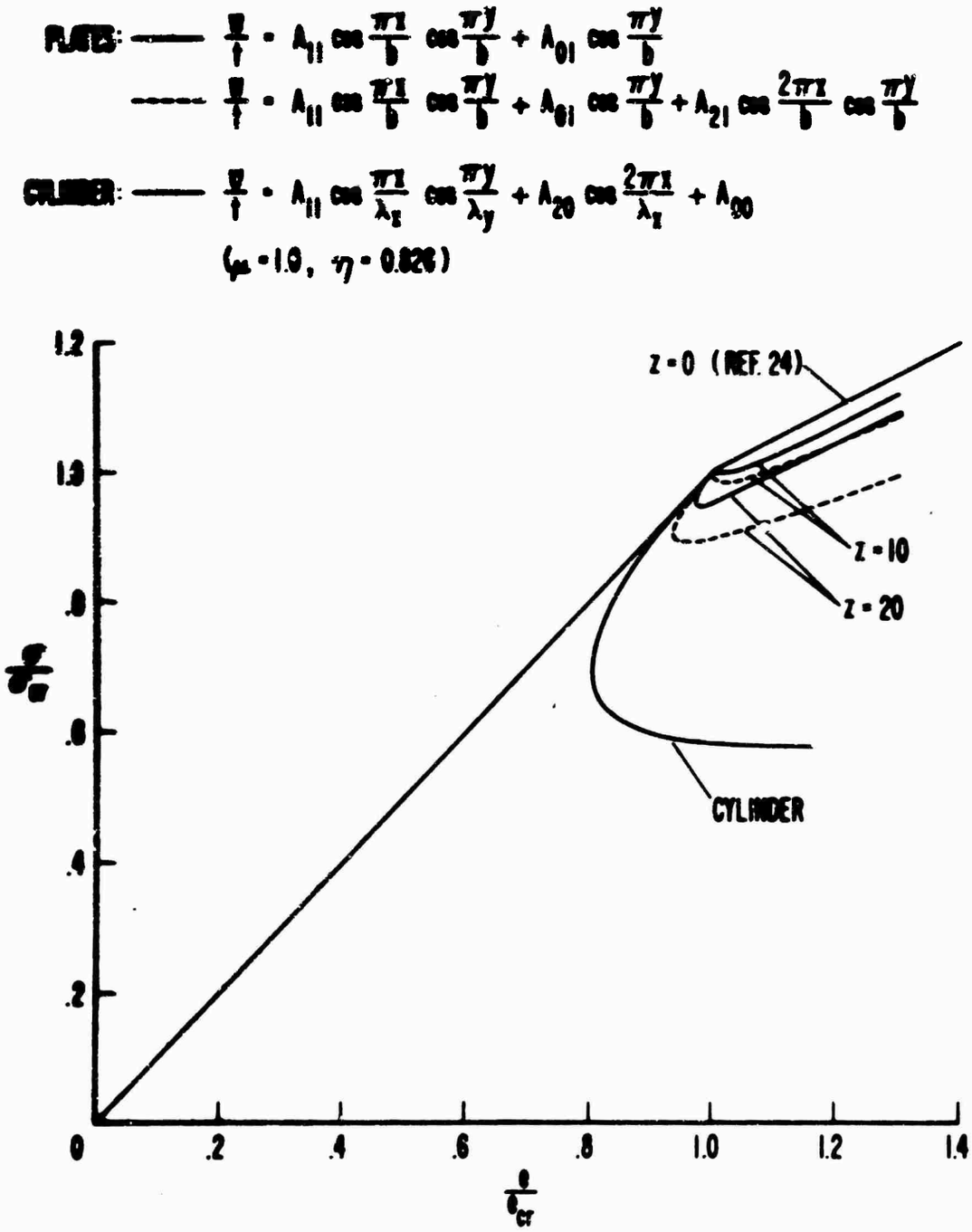

Figure 6. Average Stress-Unit End Shortening Curves for Flat and Curved Plates Covering the Range $0 \leq Z \leq \infty$.

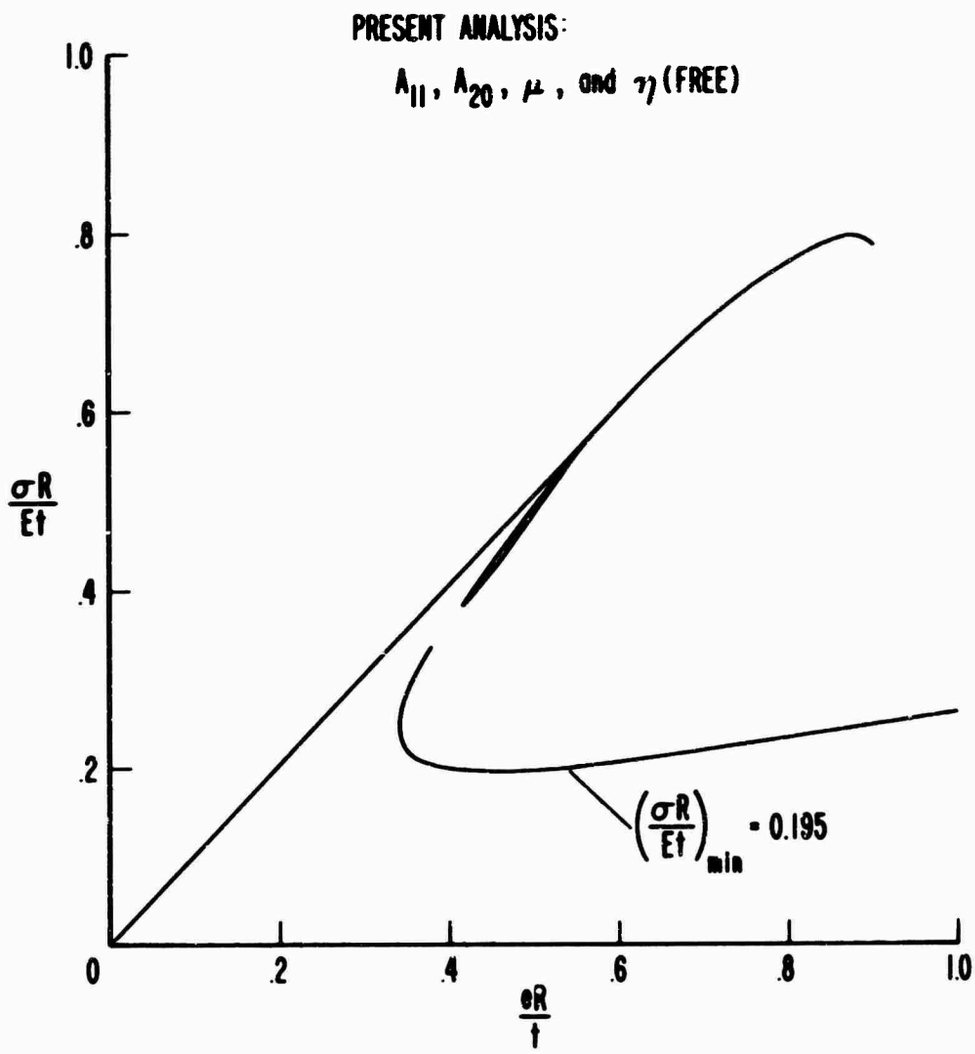

Figure 7. Average Stress-Unit End Shortening Curve for Modified-Kempner Radial Deflection Function ($A_{02} = 0$).

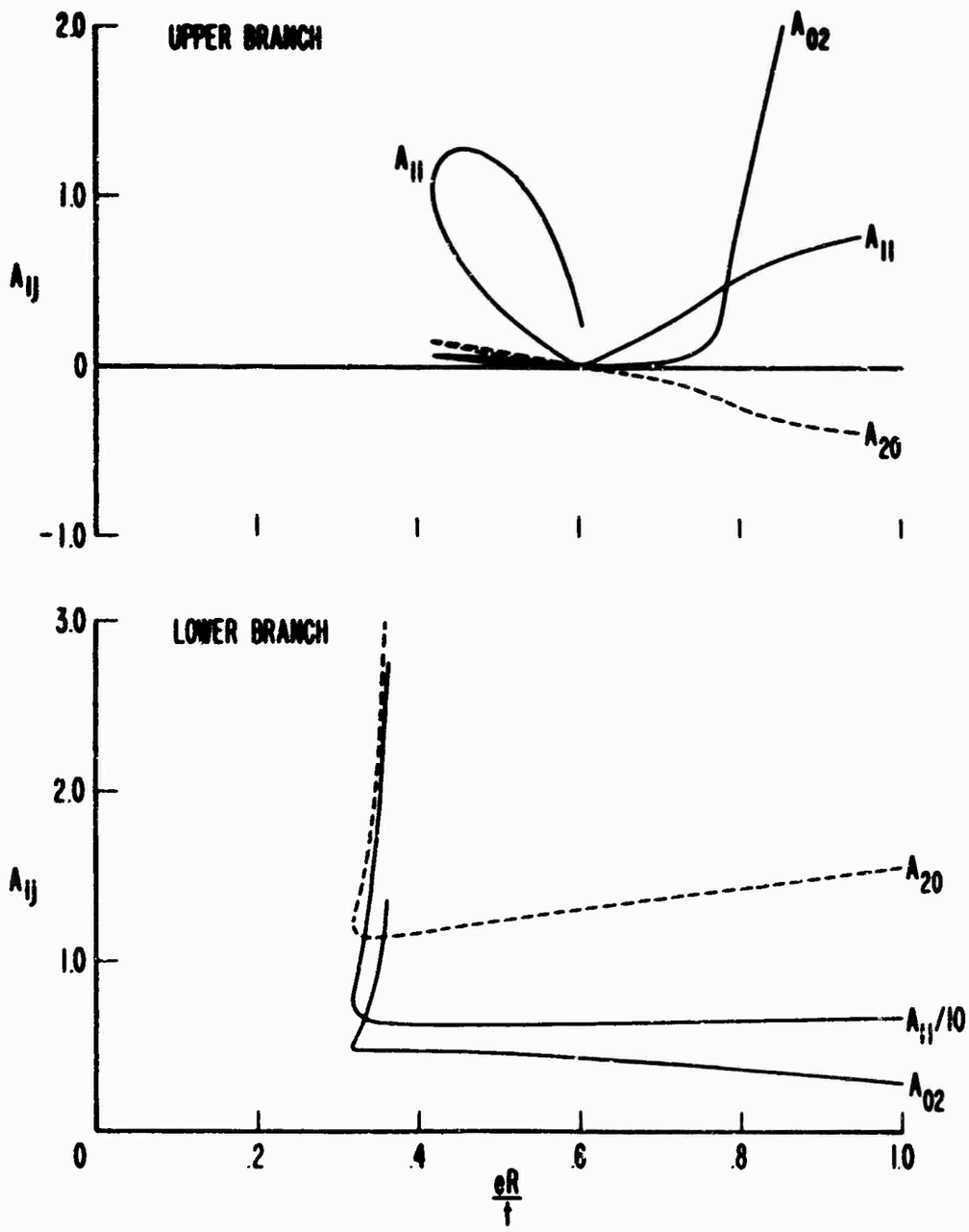

Figure 8. Variation of Radial Deflection Pattern Amplitudes A_{11}, A_{20}, and A_{02} With Unit End Shortening for Present Analysis Solution Corresponding to Kempner Deflection Function.

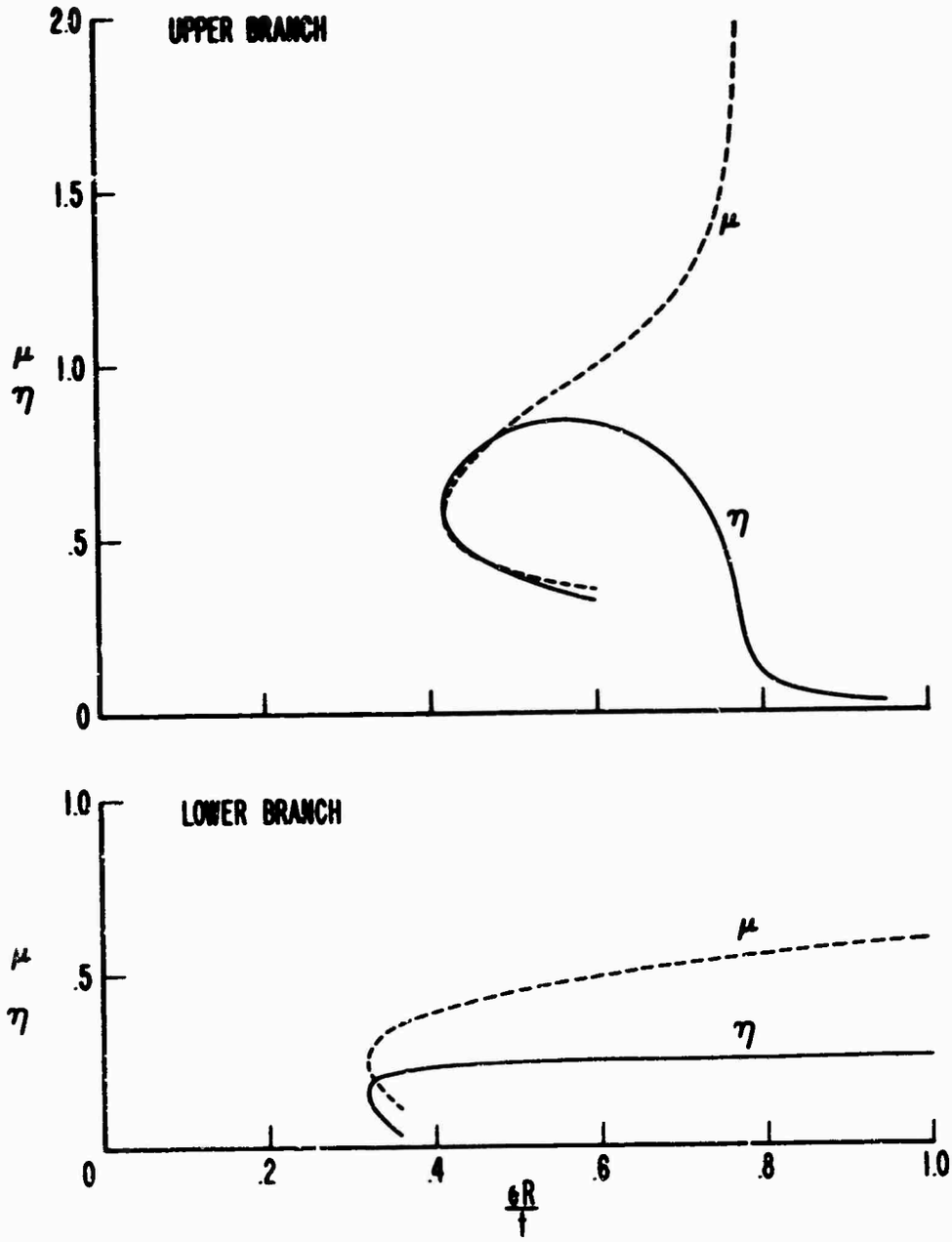

Figure 9. Variation of Radial Deflection Pattern Wave Parameters μ and η With Unit End Shortening for Present Analysis Solution Corresponding to Kempner Deflection Function.

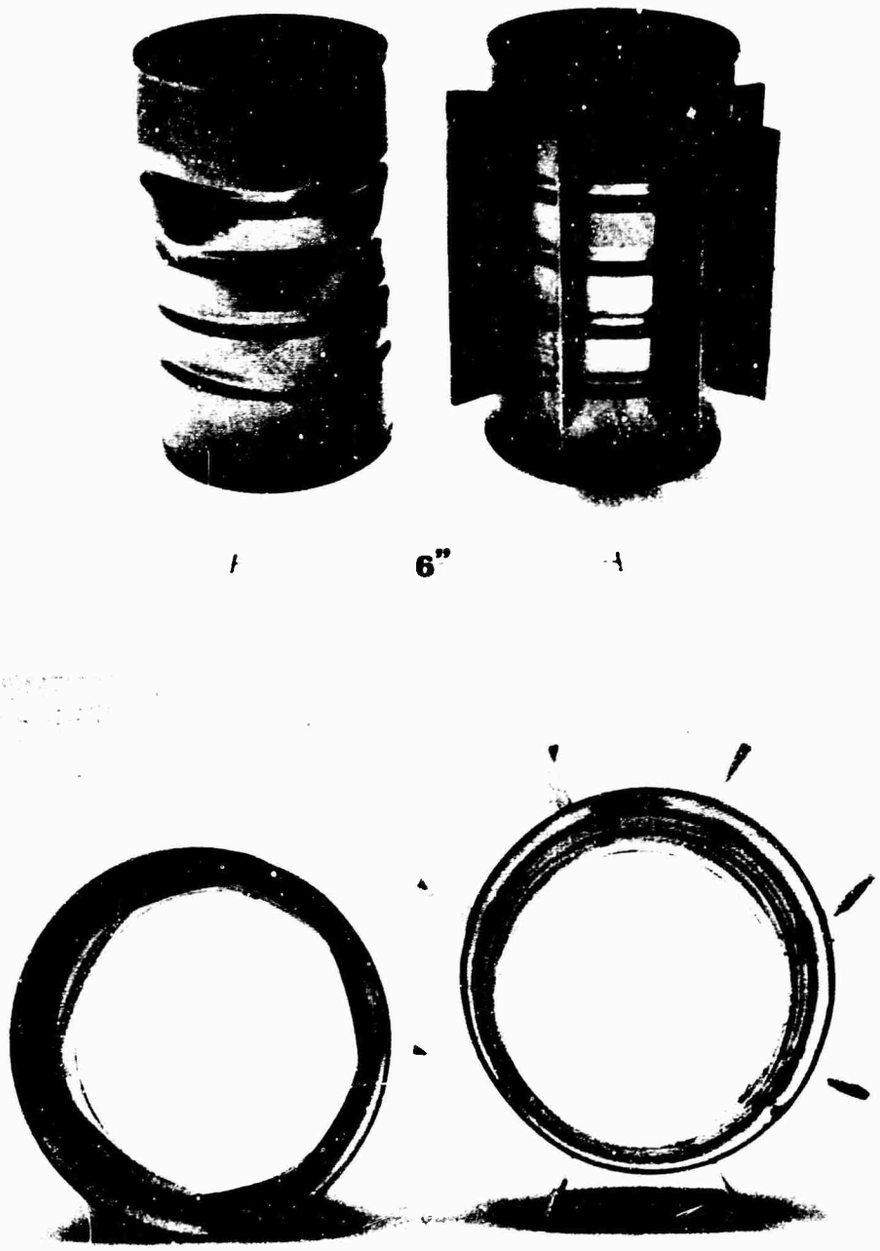

Figure 10. Effect of Lightweight Longitudinal Stiffeners in Preventing Catastrophic Snap-Through Buckling Into a Yoshimura Pattern.

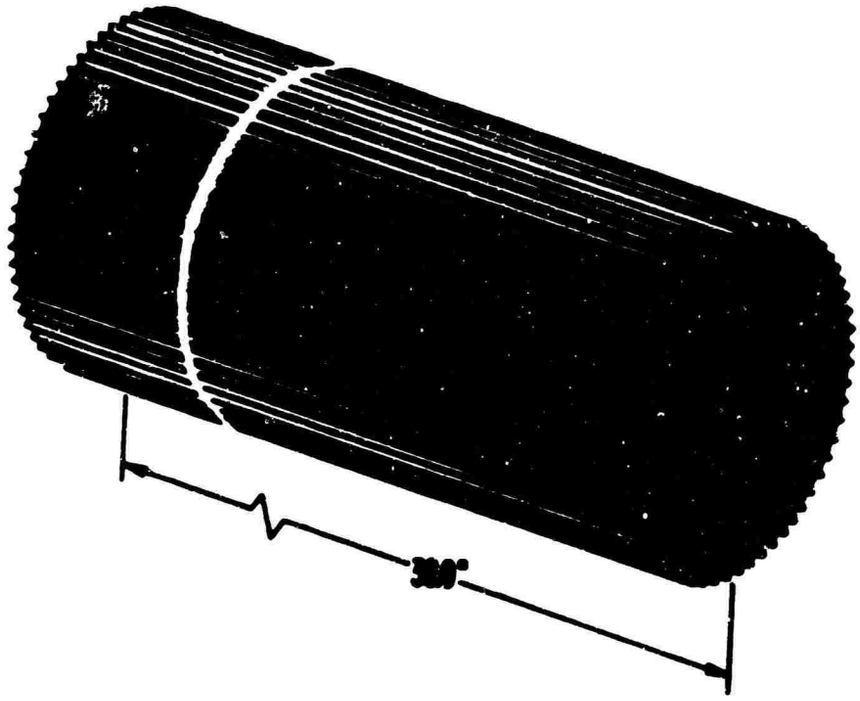

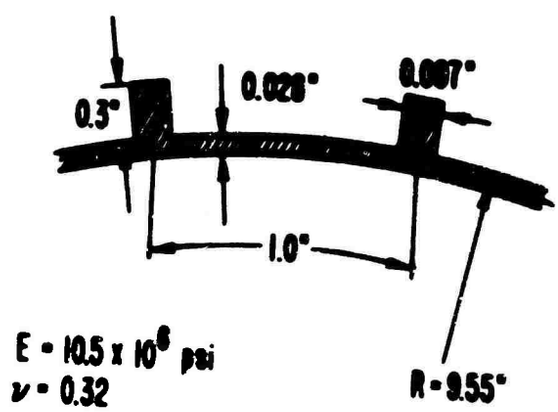

Figure 11. Physical Properties of Stiffened Shell Used as a Basis for Optimizing Procedure.

LITERATURE CITED

1. Lorenz, Rudolf, ACHSENSYMMETRISCHE VERZERRUNGEN IN DÜNNWANANDIGEN HOHLZYLINDERN, Zeitschrift des Vereines Deutcher Ingenieure, Vol. 52, No. 43, October 1908, p. 1706.

2. Timoshenko, S., EINIGE STABILITÄTSPROBLEME DER ELASTIZITÄTSTHEORIE, Zeitschrift für Mathematick und Physik, Vol. 58, No. 4, June 1910, p. 337.

3. Southwell, R. V., ON THE GENERAL THEORY OF ELASTIC STABILITY, Philosophical Transactions of the Royal Society, London, Series A, Vol. 13, No. A501, August 1913, p. 187.

4. Hoff, N. J., THIN SHELLS IN AEROSPACE STRUCTURES, Fourth von Kármán Lecture Presented at the Third AIAA Annual Meeting, November 29, 1966. Aeronautics and Astronautics, Feb. 1967, pp. 26-45.

5. Hoff, N. J., THE PERPLEXING BEHAVIOR OF THIN CIRCULAR CYLINDRICAL SHELLS IN AXIAL COMPRESSION, Second Theodore von Karman Memorial Lecture of the Israel Society of Aeronautical Sciences, Israel Journal of Technology, Vol. 4, No. 1, 1966, pp. 1-28.

6. Stein, M., RECENT ADVANCES IN THE INVESTIGATION OF SHELL BUCKLING, AIAA Journal, Vol. 6, No. 12, December 1968, pp. 2339-2345.

7. Donnell, L. H., A NEW THEORY FOR THE BUCKLING OF THIN CYLINDERS UNDER AXIAL COMPRESSION AND BENDING, Transactions of the American Society of Mechanical Engineers, Vol. 56, No. 11, November 1934, pp. 795-806.

8. Von Kármán, Theodore, and Tsien, H. S., THE BUCKLING OF THIN CYLINDRICAL SHELLS UNDER AXIAL COMPRESSION, Journal of the Aeronautical Sciences, Vol. 8, No. 8, June 1941, pp. 303-312.

9. Leggett, D. M. A., and Jones, R. P. N., THE BEHAVIOR OF A CYLINDRICAL SHELL UNDER AXIAL COMPRESSION WHEN THE BUCKLING LOAD HAS BEEN EXCEEDED, Aeronautical Research Council Reports and Memoranda, No. 2190, August 1942.

10. Michielsen, Herman F., THE BEHAVIOR OF THIN CYLINDRICAL SHELLS AFTER BUCKLING UNDER AXIAL COMPRESSION, Journal of the Aeronautical Sciences, Vol. 15, No. 12, December 1948, pp. 738-744.

11. Donnell, L. H., and Wan, C. C., EFFECT OF IMPERFECTIONS ON BUCKLING OF THIN CYLINDERS AND COLUMNS UNDER AXIAL COMPRESSION, Journal of Applied Mechanics, Vol. 17, No. 1, March 1950, pp. 73-83.

12. Madsen, W. A., and Hoff, N. J., THE SNAP-THROUGH AND POSTBUCKLING EQUILIBRIUM BEHAVIOR OF CIRCULAR CYLINDRICAL SHELLS UNDER AXIAL LOAD, Stanford University Department of Aeronautics and Astronautics, SUDAER No. 227, April 1965.

13. Kempner, J., POSTBUCKLING BEHAVIOR OF AXIALLY COMPRESSED CIRCULAR CYLINDRICAL SHELLS, Journal of the Aeronautical Sciences, Vol. 17, No. 5, May 1954, pp. 329-335, 342.

14. Almroth, B. O., POSTBUCKLING BEHAVIOR OF AXIALLY COMPRESSED CIRCULAR CYLINDERS, AIAA Journal, Vol. 1, No. 3, March 1963, pp. 630-633.

15. Hoff, N. J., Madsen, W. A., and Mayers J., THE POSTBUCKLING EQUILIBRIUM OF AXIALLY COMPRESSED CIRCULAR CYLINDRICAL SHELLS, AIAA Journal, Vol. 4, No. 1, January 1966, pp. 126 133.

16. Mayers, J., and Rehfield, L. W., DEVELOPMENTS IN MECHANICS, Vol. 3, Part 1, (Proceedings of the Ninth Midwestern Mechanics Conference, Madison, Wisconsin, August 16-18, 1965), New York, John Wiley and Sons, Inc., 1967, pp. 145-160.

17. Yoshimura, Y., ON THE MECHANISM OF BUCKLING OF A CIRCULAR CYLINDRICAL SHELL UNDER AXIAL COMPRESSION, NACA Technical Memorandum 1390, National Advisory Committee for Aeronautics, July 1955.

18. Tennyson, R. C., and Welles, S. W., ANALYSIS OF THE BUCKLING PROCESS OF CIRCULAR CYLINDRICAL SHELLS UNDER AXIAL COMPRESSION, University of Toronto; Institute of Aerospace Studies, UTIAS Report No. 129 February 1968. (In process of publication in AIAA Journal.)

19. Mayers, J., and Wrenn, B. G., DEVELOPMENTS IN MECHANICS, Vol. 4, (Proceedings of the Tenth Midwestern Mechanics Conference, Fort Collins, Colorado, August 21-23, 1967), Johnson Publishing Co., 1968, pp. 819-846.

20. Mayers, J., and Budiansky, B., ANALYSIS OF BEHAVIOR OF SIMPLY SUPPORTED FLAT PLATES COMPRESSED BEYOND BUCKLING INTO THE PLASTIC RANGE, NACA Technical Note 3368, National Advisory Committee for Aeronautics, February 1955.

21. Hu, P. C., Lundquist, E. E., and Batdorf, S. B., EFFECT OF SMALL DEVIATIONS FROM FLATNESS ON EFFECTIVE WIDTH AND BUCKLING OF PLATES IN COMPRESSION, NACA Technical Note 1124, National Advisory Committee for Aeronautics, September 1946.

22. Loo, T. T., EFFECTS OF LARGE DEFLECTIONS AND IMPERFECTIONS ON THE ELASTIC BUCKLING OF CYLINDERS UNDER TORSION AND AXIAL COMPRESSION, (Proceedings of the Second U. S. Congress of Applied Mechanics, Ann Arbor, Michigan, June 14-18, 1954), New York, The American Society of Mechanical Engineers, 1954, pp. 345-357.

23. Thielemann, W., NEW DEVELOPMENTS IN THE NONLINEAR THEORIES OF BUCKLING OF THIN CYLINDRICAL SHELLS, (Proceedings of the Durand Centennial Conference, Stanford, California, August 5-8, 1959), New York, Pergamon Press, 1960, pp. 76-119.

24. Mayers, J., and Wesenberg, D. L., THE MAXIMUM STRENGTH OF INITIALLY IMPERFECT, AXIALLY COMPRESSED, CIRCULAR CYLINDRICAL SHELLS, Stanford University; USAAVLABS Technical Report 69-60, U. S. Army Aviation Materiel Laboratories, Fort Eustis, Virginia, August 1969. Presented at the AIAA 7th Aerospace Sciences Meeting, AIAA Paper No. 69-61, New York, January 1969.

25. Mayers, J. and Nelson, E., MAXIMUM STRENGTH ANALYSIS OF POSTBUCKLED RECTANGULAR PLATES, Stanford University; USAAVLABS Technical Report 69-64, U. S. Army Aviation Materiel Laboratories, Fort Eustis, Virginia (in publication). Presented at the AIAA 6th Aerospace Sciences Meeting, AIAA Paper No. 68-171, New York, January 1968.

26. Smith, G. W., and Spier, E. E., THE STABILITY OF ECCENTRICALLY STIFFENED CIRCULAR CYLINDERS, VOLUME I – GENERAL, Convair Division of General Dynamics, Report No. GDC DDG 67-006, June 1967.

27. Baker, E. H., Capelli, A. P., Kovalevsky, L., Rish, F. L., and Verette, R. M., SHELL ANALYSIS MANUAL, NASA CR-912, National Aeronautics and Space Administration, April 1968.

28. Card, M. F., and Jones, R. M., EXPERIMENTAL AND THEORETICAL RESULTS FOR BUCKLING OF ECCENTRICALLY STIFFENED CYLINDERS, NASA Technical Note D-3639, National Aeronautics and Space Administration, Oct. 1966.

29. Schildcrout, M., and Stein, M., CRITICAL AXIAL-COMPRESSIVE STRESS OF A CURVED RECTANGULAR PANEL WITH A CENTRAL LONGITUDINAL STIFFENER, NACA Technical Note 1661, National Advisory Committee for Aeronautics, July 1948.

30. Batdorf, S. B., and Schildcrout, M., CRITICAL AXIAL-COMPRESSIVE STRESS OF A CURVED RECTANGULAR PANEL WITH A CENTRAL CHORDWISE STIFFENER, NACA Technical Note 1879, National Advisory Committee for Aeronautics, May 1949.

31. Block, D. L., Card, M. F., and Mikulas, M. M., Jr., BUCKLING OF ECCENTRICALLY STIFFENED ORTHOTROPIC CYLINDERS, NASA Technical Note D-2960, National Aeronautics and Space Administration, August 1965.

32. Anonymous, BUCKLING OF THIN-WALLED CIRCULAR CYLINDERS, NASA SP-8007, National Aeronautics and Space Administration, August 1968.

33. Smith, G. W., and Spier, E. E., THE STABILITY OF ECCENTRICALLY STIFFENED CIRCULAR CYLINDERS, VOLUME V - EFFECTS OF INITIAL IMPERFECTIONS; AXIAL COMPRESSION AND PURE BENDING, Convair Division of General Dynamics Report No. GDC DDG 67-006, June 1967.

APPENDIX I

DEVELOPMENT OF GOVERNING EQUATIONS AND BOUNDARY CONDITIONS

The total potential energy, equation (8), upon substitution of the strains given by equation (5), and subsequent integration through the shell thickness, gives in expanded form

$$
\begin{aligned}
U = \frac{Et}{(1-\nu^2)} \int_{-L/2}^{L/2}\int_0^{2\pi R} [(&\tfrac{1}{2} u_{,x}^2 + \tfrac{1}{8} w_{,x}^4 + \tfrac{1}{2} w_{,x}^2 w_{0,x}^2 + \tfrac{1}{2} v_{,y}^2 + \tfrac{1}{8} w_{,y}^4 + \tfrac{1}{2} w_{,y}^2 w_{0,y}^2 \\
&+ \frac{1}{2R^2} w^2 + \tfrac{1}{2} u_{,x} w_{,x}^2 + u_{,x} w_{,x} w_{0,x} + u_{,x} v_{,y} + \tfrac{1}{2} u_{,x} w_{,y}^2 + u_{,x} w_{,y} w_{0,y} - \tfrac{1}{R} u_{,x} w \\
&+ \tfrac{1}{2} w_{,x}^3 w_{0,x} + \tfrac{1}{2} v_{,y} w_{,x}^2 + \tfrac{1}{4} w_{,x}^2 w_{,y}^2 + \tfrac{1}{2} w_{,x}^2 w_{,y} w_{0,y} - \tfrac{1}{2R} w_{,x}^2 w + v_{,y} w_{,x} w_{0,x} \\
&+ \tfrac{1}{2} w_{,x} w_{,y}^2 w_{0,x} + w_{,x} w_{,y} w_{0,x} w_{0,y} - \tfrac{1}{R} w_{,x} w_{0,x} w + \tfrac{1}{2} v_{,y} w_{,y}^2 + v_{,y} w_{,y} w_{0,y} \\
&- \tfrac{1}{R} v_{,y} w + \tfrac{1}{2} w_{,y}^3 w_{0,y} - \tfrac{1}{2R} w_{,y}^2 w - \tfrac{1}{R} w_{,y} w_{0,y} w) - (1-\nu)(u_{,x} v_{,y} + \tfrac{1}{2} u_{,x} w_{,y}^2 \\
&+ u_{,x} w_{,y} w_{0,y} - \tfrac{1}{R} u_{,x} w + \tfrac{1}{2} w_{,x}^2 v_{,y} - \tfrac{1}{2R} w_{,x}^2 w + w_{,x} w_{0,x} v_{,y} + \tfrac{1}{2} w_{,x} w_{0,x} w_{,y} w_{0,y} \\
&- \tfrac{1}{R} w_{,x} w_{0,x} w - \tfrac{1}{4} u_{,y}^2 - \tfrac{1}{4} v_{,x}^2 - \tfrac{1}{4} w_{0,x}^2 w_{,y}^2 - \tfrac{1}{4} w_{,x}^2 w_{0,y}^2 - \tfrac{1}{2} u_{,y} v_{,x} - \tfrac{1}{2} u_{,y} w_{,x} w_{,y} \\
&- \tfrac{1}{2} u_{,y} w_{0,x} w_{,y} - \tfrac{1}{2} u_{,y} w_{,x} w_{0,y} - \tfrac{1}{2} v_{,x} w_{,x} w_{,y} - \tfrac{1}{2} v_{,x} w_{0,x} w_{,y} \\
&- \tfrac{1}{2} v_{,x} w_{,x} w_{0,y})]\,dx\,dy + \frac{D}{2} \int_{-L/2}^{L/2}\int_0^{2\pi R} [(w_{,xx} + w_{,yy})^2 \\
&- 2(1-\nu)(w_{,xx} w_{,yy} - w_{,xy}^2)]\,dx\,dy
\end{aligned}
\tag{29}
$$

In accordance with the potential energy principle, the first variation of the strain functional, equation (29), with respect to the displacements u, v, and w must vanish. Thus,

$$\delta_{u,v,w}(U) = \frac{Et}{(1-\nu^2)} \int_{-L/2}^{L/2}\int_0^{2\pi R} \Big\{[(u,_x+\tfrac{1}{2}w,_x^2+w,_xw_{0,x})$$

$$+ \nu(v,_y+\tfrac{1}{2}w,_y^2+w,_yw_{0,y} - \tfrac{w}{R})]\delta u,_x + \frac{(1-\nu)}{2}(u,_y+v,_x+w,_xw,_y+w_{0,x}w,_y$$

$$+ w,_xw_{0,y})(\delta u,_y+\delta v,_x) + [(u,_y+\tfrac{1}{2}w,_y^2+w,_yw_{0,y}-\tfrac{w}{R}) + \nu(u,_x+\tfrac{1}{2}w,_x^2$$

$$+ w,_xw_{0,x})]\delta v,_y + \{(w,_x+w_{0,x})[(u,_x+\tfrac{1}{2}w,_x^2+w,_xw_{0,x}) + \nu(v,_y+\tfrac{1}{2}w,_y^2$$

$$+ w,_yw_{0,y}-\tfrac{w}{R})] + \frac{(1-\nu)}{2}(w,_y+w_{0,y})(u,_y+v,_x+w,_xw,_y+w_{0,x}w,_y$$

$$+ w,_xw_{0,y})\}\delta w,_x + \{(w,_y+w_{0,y})[(v,_y+\tfrac{1}{2}w,_y^2+w,_yw_{0,y}-\tfrac{w}{R}) + \nu(u,_x$$

$$+ \tfrac{1}{2}w,_x^2+w,_xw_{0,x})] + \frac{(1-\nu)}{2}(w,_x+w_{0,x})(u,_y+v,_x+w,_xw,_y+w_{0,x}w,_y$$

$$+ w,_xw_{0,y})\}\delta w,_y - \frac{1}{R}[(v,_y+\tfrac{1}{2}w,_y^2+w,_yw_{0,y}-\tfrac{w}{R}) + \nu(u,_x+\tfrac{1}{2}w,_x^2$$

$$+ w,_xw_{0,x})]\delta w\Big\}\,dxdy + D\int_{-L/2}^{L/2}\int_0^{2\pi R}[(w,_{xx}+w,_{yy})\delta w,_{xx}$$

$$+ (w,_{yy}+\nu w,_{xx})\delta w,_{yy}+2(1-\nu)w,_{xy}\delta w,_{xy}]dxdy = 0 \qquad (30)$$

Integration by parts followed by appropriate grouping of terms yields

$$\delta_{u,v,w}(U) = -\frac{Et}{(1-\nu^2)} \int_{-L/2}^{L/2}\int_0^{2\pi R} \Big\{[(u,_x+\tfrac{1}{2}w,_x^2+w,_xw_{0,x})+$$

$$+ \nu(v,_y+\tfrac{1}{2}w,_y^2+w,_yw_{0,y} - \tfrac{w}{R})],_x\delta u + \frac{(1-\nu)}{2}(u,_y+v,_x+w,_xw,_y+w_{0,x}w,_y$$

$$+ w,_xw_{0,y}),_y\delta u + [(v,_y+\tfrac{1}{2}w,_y^2+w,_yw_{0,y}-\tfrac{w}{R}) + \nu(u,_x+\tfrac{1}{2}w,_x^2+w,_xw_{0,x})],_y\delta v$$

(continued)

$$+ \frac{(1-\nu)}{2}(u_{,y}+v_{,x}+w_{,x}w_{,y}+w_{0,x}w_{,y}+w_{,x}w_{0,y})_{,x}\delta v + (w_{,x}+w_{0,x})\{[(u_{,x}$$

$$+ \frac{1}{2}w_{,x}^2+w_{,x}w_{0,x}) + \nu(v_{,y}+\frac{1}{2}w_{,y}^2+w_{,y}w_{0,y}-\frac{w}{R})]_{,x} + \frac{(1-\nu)}{2}(u_{,y}+v_{,x}$$

$$+ w_{,x}w_{,y}+w_{0,x}w_{,y}+w_{,x}w_{0,y})_{,y}\}\delta w + (w_{,y}+w_{0,y})\{[(v_{,y}+\frac{1}{2}w_{,y}^2+w_{,y}w_{0,y}-\frac{w}{R})$$

$$+ \nu(u_{,x}+\frac{1}{2}w_{,x}^2+w_{,x}w_{0,x})]_{,y} + \frac{(1-\nu)}{2}(u_{,y}+v_{,x}+w_{,x}w_{,y}+w_{0,x}w_{,y}$$

$$+ w_{,x}w_{0,y})_{,x}\} + (w_{,x}+w_{0,x})_{,x}[(u_{,x}+\frac{1}{2}w_{,x}^2+w_{,x}w_{0,x}) + \nu(v_{,y}+\frac{1}{2}w_{,y}^2$$

$$+ w_{,y}w_{0,y}-\frac{w}{R})]\delta w + (w_{,y}+w_{0,y})_{,y}[(v_{,y}+\frac{1}{2}w_{,y}^2+w_{,y}w_{0,y}-\frac{w}{R}) + \nu(u_{,x}$$

$$+ \frac{1}{2}w_{,x}^2+w_{,x}w_{0,x})]\delta w + \frac{(1-\nu)}{2}[(w_{,x}+w_{0,x})_{,y}+(w_{,y}+w_{0,y})_{,x}](u_{,y}+v_{,x}$$

$$+ w_{,x}w_{,y}+w_{0,x}w_{,y}+w_{,x}w_{0,y})\delta w + \frac{1}{R}[(v_{,y}+\frac{1}{2}w_{,y}^2+w_{,y}w_{0,y}-\frac{w}{R}) + \nu(u_{,x}+\frac{1}{2}w_{,x}^2$$

$$+ w_{,x}w_{0,x})]\delta w\Big\} dxdy + D\int_{-L/2}^{L/2}\int_0^{2\pi R}\nabla^4 w\delta w dxdy + \frac{Et}{(1-\nu^2)}\int_0^{2\pi R}[(u_{,x}$$

$$+ \frac{1}{2}w_{,x}^2+w_{,x}w_{0,x}) + \nu(v_{,y}+\frac{1}{2}w_{,y}^2+w_{,y}w_{0,y}-\frac{w}{R})]\delta u\Big|_{-L/2}^{L/2} dy$$

$$+ \frac{Et}{2(1+\nu)}\int_{-L/2}^{L/2}(u_{,y}+v_{,x}+w_{,x}w_{,y}+w_{0,x}w_{,y}+w_{,x}w_{0,y})\delta u\Big|_0^{2\pi R} dx$$

$$+ \frac{Et}{2(1+\nu)}\int_0^{2\pi R}(u_{,y}+v_{,x}+w_{,x}w_{,y}+w_{0,x}w_{,y}+w_{,x}w_{0,y})\delta v\Big|_{-L/2}^{L/2} dy$$

$$+ \frac{Et}{(1-\nu^2)}\int_{-L/2}^{L/2}[(v_{,y}+\frac{1}{2}w_{,y}^2+w_{,y}w_{0,y}-\frac{w}{R}) + \nu(u_{,x}+\frac{1}{2}w_{,x}^2+w_{,x}w_{0,x})]\delta v\Big|_0^{2\pi R} dx$$

$$+ D\int_{-L/2}^{L/2}(w_{,yy}+\nu w_{,xx})\delta w_{,y}\Big|_0^{2\pi R} dx + D\int_0^{2\pi R}(w_{,xx}+\nu w_{,yy})\delta w_{,x}\Big|_{-L/2}^{L/2} dy$$

(continued)

$$- D \int_{-L/2}^{L/2} [w_{,yyy}+(2-\nu)w_{,xxy}]\delta w \Big|_0^{2\pi R} dx - D \int_0^{2\pi R} \{w_{,xxx}$$

$$+ (2-\nu)w_{,xyy}]\delta w \Big|_{-L/2}^{L/2} dy + \frac{Et}{(1-\nu^2)} \int_{-L/2}^{L/2} \{(w_{,y}+w_{0,y})[(v_{,y}+\frac{1}{2}w_{,y}^2+w_{,y}w_{0,y}$$

$$- \frac{w}{R}) + \nu(u_{,x}+\frac{1}{2}w_{,x}^2+w_{,x}w_{0,x})] + \frac{(1-\nu)}{2}(w_{,x}+w_{0,x})(u_{,y}+v_{,x}+w_{,x}w_{,y}$$

$$+ w_{0,x}w_{,y}+w_{,x}w_{0,y})]\delta w \Big|_0^{2\pi R} dx + \frac{Et}{(1-\nu^2)} \int_0^{2\pi R} \{(w_{,x}+w_{0,x})[(u_{,x}$$

$$+ \frac{1}{2}w_{,x}^2+w_{,x}w_{0,x}) + \nu(v_{,y}+\frac{1}{2}w_{,y}^2+w_{,y}w_{0,y}-\frac{w}{R})] + \frac{(1-\nu)}{2}(u_{,y}+v_{,x}$$

$$+ w_{,x}w_{,y}+w_{0,x}w_{,y}+w_{,x}w_{0,y})(w_{,y}+w_{0,y})\}\delta w \Big|_{-L/2}^{L/2} dy + 2D(1-\nu)w_{,xy}\delta w \Big|_0^{2\pi R} \Big|_{-L/2}^{L/2}$$

$$= 0 \tag{31}$$

With the use of the strain-displacement relations, equation (3), equation (31) can be rewritten as

$$\delta_{u,v,w}(U) = - \frac{Et}{(1-\nu^2)} \int_{-L/2}^{L/2}\int_0^{2\pi R} \Big\{[(\epsilon_x^0+\nu\epsilon_y^0)_{,x} + \frac{(1-\nu)}{2}\gamma_{xy,y}^0]\delta u$$

$$+ [(\epsilon_y^0+\nu\epsilon_x^0)_{,y}+\frac{(1-\nu)}{2}\gamma_{xy,x}^0]\delta v + \{(w_{,x}+w_{0,x})[(\epsilon_x^0+\nu\epsilon_y^0)_{,x} + \frac{(1-\nu)}{2}\gamma_{xy,y}^0]$$

$$+ (w_{,y}+w_{0,y})[(\epsilon_y^0+\nu\epsilon_x^0)_{,y} + \frac{(1-\nu)}{2}\gamma_{xy,x}^0] + (\epsilon_x^0+\nu\epsilon_y^0)(w_{,x}+w_{0,x})_{,x}$$

$$+ (\epsilon_y^0+\nu\epsilon_x^0)(w_{,y}+w_{0,y})_{,y} + (1-\nu)\gamma_{xy}^0(w_{,x}+w_{0,x})_{,y} + \frac{1}{R}(\epsilon_y^0+\nu\epsilon_x^0)\}\delta w\Big\} dxdy$$

$$+ D \int_{-L/2}^{L/2}\int_0^{2\pi R} \nabla^4 w\delta w dxdy + \frac{Et}{(1-\nu^2)} \int_0^{2\pi R} (\epsilon_x^0+\nu\epsilon_y^0)\delta u \Big|_{-L/2}^{L/2} dy$$

$$+ \frac{Et}{2(1+\nu)} \int_{-L/2}^{L/2} \gamma_{xy}^0 \delta u \Big|_0^{2\pi R} dx + \frac{Et}{(1-\nu^2)} \int_{-L/2}^{L/2} (\epsilon_y^0+\nu\epsilon_x^0)\delta v \Big|_0^{2\pi R} dx$$

(continued)

$$+ \frac{Et}{2(1+\nu)} \int_0^{2\pi R} \gamma_{xy}^0 \delta v \Big|_{-L/2}^{L/2} dy + D \int_{-L/2}^{L/2} (w_{,yy} + \nu w_{,xx}) \delta w_{,y} \Big|_0^{2\pi R} dx$$

$$+ D \int_0^{2\pi R} (w_{,xx} + \nu w_{,yy}) \delta w_{,x} \Big|_{-L/2}^{L/2} dy - D \int_{-L/2}^{L/2} [w_{,yyy} + (2-\nu) w_{,xxy}] \delta w \Big|_0^{2\pi R} dx$$

$$- D \int_0^{2\pi R} [w_{,xxx} + (2-\nu) w_{,xyy}] \delta w \Big|_{-L/2}^{L/2} dy + \frac{Et}{(1-\nu^2)} \int_{-L/2}^{L/2} [(w_{,y} + w_{0,y})(\epsilon_y^0 + \nu \epsilon_x^0)$$

$$+ \frac{(1-\nu)}{2} (w_{,x} + w_{0,x}) \gamma_{xy}^0] \delta w \Big|_0^{2\pi R} dx + \frac{Et}{(1-\nu^2)} \int_0^{2\pi R} [(w_{,x} + w_{0,x})(\epsilon_x^0 + \nu \epsilon_y^0)$$

$$+ \frac{(1-\nu)}{2} (w_{,y} + w_{0,y}) \gamma_{xy}^0] \delta w \Big|_{-L/2}^{L/2} dy + 2D(1-\nu) w_{,xy} \delta w \Big|_0^{2\pi R} \Big|_{-L/2}^{L/2} = 0 \qquad (32)$$

Now, with the introduction of the stress-strain relations (equations (6)), written for the middle surface, the variation of the total potential energy with respect to the displacements u, v, and w is expressed as

$$\delta_{u,v,w}(U) = -\int_{-L/2}^{L/2} \int_0^{2\pi R} \{(N_{x,x}^0 + N_{xy,y}^0) \delta u + (N_{y,y}^0 + N_{xy,x}^0) \delta v$$

$$+ [(w_{,x} + w_{0,x})(N_{x,x}^0 + N_{xy,y}^0) + (w_{,y} + w_{0,y})(N_{y,y}^0 + N_{xy,x}^0) + N_x^0 (w_{,x} + w_{0,x})_{,x}$$

$$+ N_y^0 (w_{,y} + w_{0,y})_{,y} + 2N_{xy}^0 (w_{,x} + w_{0,x})_{,y} + \frac{1}{R} N_y^0 - D\nabla^4 w] \delta w\} dx dy$$

$$+ \int_{-L/2}^{L/2} \{N_{xy}^0 \delta u + N_y^0 \delta v + [N_y^0 (w_{,y} + w_{0,y}) + N_{xy}^0 (w_{,x} + w_{0,x}) + M_{y,y}$$

$$+ 2M_{xy,x}] \delta w\} \Big|_0^{2\pi R} dx + \int_0^{2\pi R} \{N_x^0 \delta u + N_{xy}^0 \delta v + [N_x^0 (x_{,x} + w_{0,x})$$

$$+ N_{xy}^0 (w_{,y} + w_{0,y}) + M_{x,x} + 2M_{xy,y}] \delta w\} \Big|_{-L/2}^{L/2} dy - \int_{-L/2}^{L/2} M_y \delta w_{,y} \Big|_0^{2\pi R} dx$$

$$- \int_0^{2\pi R} M_x \delta w_{,x} \Big|_{-L/2}^{L/2} dy + 2D(1-\nu) w_{,xy} \delta w \Big|_0^{2\pi R} \Big|_{-L/2}^{L/2} = 0 \qquad (33)$$

Finally, since the generalized displacements are arbitrary in the interior of the shell and at the boundaries, as appropriate, equation (33) yields the equilibrium equations

$$\left.\begin{aligned}
&N^0_{x,x} + N^0_{xy,y} = 0 \\
&N^0_{y,y} + N^0_{xy,x} = 0 \\
&D\nabla^4 w - N^0_x(w_{,x}+w_{0,x})_{,x} - N^0_y(w_{,y}+w_{0,y})_{,y} - 2N^0_{xy}(w_{,x}+w_{0,x})_{,y} - \frac{1}{R}N^0_y = 0
\end{aligned}\right\} \quad (34)$$

(where the first two relations of equation (34) have been used to simplify the third), and the attendant boundary conditions at

$x = \pm \frac{L}{2}$:

$$\left.\begin{aligned}
&\int_0^{2\pi R} N^0_x dy = 0 && \text{or} \quad \delta u = 0 \\
&\int_0^{2\pi R} N^0_{xy} dy = 0 && \text{or} \quad \delta v = 0 \\
&\int_0^{2\pi R} M_x dy = 0 && \text{or} \quad \delta w_{,x} = 0 \\
&\int_0^{2\pi R} [N^0_x(w_{,x}+w_{0,x})+N^0_{xy}(w_{,y}+w_{0,y})+M_{x,x}+2M_{xy,y}]dy = 0 && \text{or} \quad \delta w = 0
\end{aligned}\right\} \quad (35)$$

$y = 0, 2\pi R$:

$$\left.\begin{aligned}
&\int_{-L/2}^{L/2} N^0_y dx = 0 && \text{or} \quad \delta v = 0 \\
&\int_{-L/2}^{L/2} N^0_{xy} dx = 0 && \text{or} \quad \delta u = 0
\end{aligned}\right\}$$

(continued)

$$\left.\begin{aligned} &\int_{-L/2}^{L/2} M_y dx = 0 && \text{or} \quad \delta w_{,y} = 0 \\ &\int_{-L/2}^{L/2} [N_y^0(w_{,y}+w_{0,y})+N_{xy}^0(w_{,x}+w_{0,x})+M_{y,y}+2M_{xy,x}]dx = 0 && \text{or} \quad \delta w = 0 \end{aligned}\right\} (36)$$

$x = \pm \frac{L}{2}$, $y = 0$, $2\pi R$:

$$M_{xy} = 0 \qquad \text{or} \quad \delta w = 0 \quad (37)$$

APPENDIX II

SOLUTION OF COMPATIBILITY EQUATION

For a given trigonometric series representing the initial and buckling radial deflection shapes, the procedure for integrating the compatibility equation (24) is as follows:

Equations (21) and (23) can be rewritten as

$$\frac{w_0}{t} = A_{11}^0 \cos \mu_0 a_0 x \cos a_0 y + A_{20}^0 \cos 2\mu_0 a_0 x \tag{38}$$

and

$$\frac{w}{t} = A_{00} + A_{11} \cos \mu a x \cos a y + A_{20} \cos 2\mu a x + A_{02} \cos 2ay$$

$$+ A_{11}^* \cos \mu_0 a_0 x \cos a_0 y + A_{20}^* \cos 2\mu_0 a_0 x \tag{39}$$

where $\mu_0 = \lambda_{y_0}/\lambda_{x_0}$, $\mu = \lambda_y/\lambda_x$, $a_0 = \pi/\lambda_{y_0}$, and $a = \pi/\lambda_y$. Substitution of equations (38) and (39) into equation (24), and performance of the indicated operations, where $\nabla^{-4}\nabla^4(\ ) = 0$, yields

$$F/E = \frac{\sigma y^2}{2E} + \frac{\mu^2}{(\mu^2+1)^2}\left(\frac{tA_{11}}{Ra^2} - 2t^2 A_{11}A_{20} - 2t^2 A_{11}A_{02}\right) \cos \mu a x \cos a y$$

$$+ \frac{1}{32\mu^2}\left(\frac{8tA_{20}}{Ra^2} - t^2 A_{11}^2\right) \cos 2\mu a x - \frac{1}{32} t^2 \mu^2 A_{11}^2 \cos 2ay$$

$$- \frac{2t^2\mu^2 A_{11}A_{20}}{(9\mu^2+1)^2} \cos 3\mu a x \cos a y - \frac{2t^2\mu^2 A_{11}A_{02}}{(\mu^2+9)^2} \cos \mu a x \cos 3ay$$

$$- \frac{\mu^2 t^2 A_{20}A_{02}}{(\mu^2+1)^2} \cos 2\mu a x \cos 2ay + \frac{\mu_0^2}{(\mu_0^2+1)^2}\left[\frac{tA_{11}^*}{Ra_0^2} - 2t^2(A_{11}^* A_{20}^*\right.$$

$$\left. + A_{11}^* A_{20}^0 + A_{20}^* A_{11}^0)\right] \cos \mu_0 a_0 x \cos a_0 y + \frac{1}{32\mu_0^2}\left(\frac{8tA_{20}^*}{Ra_0^2} - t^2 A_{11}^{*2}\right.$$

(continued)

$$- 2t^2 A^*_{11} A^0_{11}\Big) \cos 2\mu_0 a_0 x - \frac{\mu_0^2 t^2}{32} (A^{*2}_{11} + 2A^*_{11} A^0_{11}) \cos 2a_0 y$$

$$- \frac{2\mu_0^2 t^2}{(9\mu_0^2+1)^2} (A^*_{11} A^*_{20} + A^*_{20} A^0_{11} + A^*_{11} A^0_{20}) \cos 3\mu_0 a_0 x \cos a_0 y$$

$$- \frac{\mu_0^2 a^2 a_0^2 t^2}{(a_0^2 \mu_0^2 + a^2)^2} A_{02} (A^*_{20} + A^0_{20}) \cos 2\mu_0 a_0 x \cos 2ay$$

$$- \frac{t^2 a^2 a_0^2 (\mu - \mu_0)^2 A_{11} (A^*_{11} + A^0_{11})}{4[(\mu a - \mu_0 a_0)^2 + (a - a_0)^2]^2} \cos (\mu a - \mu_0 a_0) x \cos (a - a_0) y$$

$$- \frac{t^2 a^2 a_0^2 (\mu - \mu_0)^2 A_{11} (A^*_{11} + A^0_{11})}{4[(\mu a + \mu_0 a_0)^2 + (a + a_0)^2]^2} \cos (\mu a + \mu_0 a_0) x \cos (a + a_0) y$$

$$- \frac{t^2 a^2 a_0^2 (\mu + \mu_0)^2 A_{11} (A^*_{11} + A^0_{11})}{4[(\mu a - \mu_0 a_0)^2 + (a + a_0)^2]^2} \cos (\mu a - \mu_0 a_0) x \cos (a + a_0) y$$

$$- \frac{t^2 a^2 a_0^2 (\mu + \mu_0)^2 A_{11} (A^*_{11} + A^0_{11})}{4[(\mu a + \mu_0 a_0)^2 + (a - a_0)^2]^2} \cos (\mu a + \mu_0 a_0) x \cos (a - a_0) y$$

$$- \frac{2t^2 a^2 a_0^2 \mu_0^2 A_{11} (A^*_{20} + A^0_{20})}{[(\mu a - 2\mu_0 a_0)^2 + a^2]^2} \cos (\mu a - 2\mu_0 a_0) x \cos ay$$

$$- \frac{2t^2 a^2 a_0^2 \mu_0^2 A_{11} (A^*_{20} + A^0_{20})}{[(\mu a + 2\mu_0 a_0)^2 + a^2]^2} \cos (\mu a + 2\mu_0 a_0) x \cos ay$$

$$- \frac{2t^2 \mu^2 a^2 a_0^2 A_{20} (A^*_{11} + A^0_{11})}{[(2\mu a - \mu_0 a_0)^2 + a_0^2]^2} \cos (2\mu a - \mu_0 a_0) x \cos a_0 y$$

$$- \frac{2t^2 \mu^2 a^2 a_0^2 A_{20} (A^*_{11} + A^0_{11})}{[(2\mu a + \mu_0 a_0)^2 + a_0^2]^2} \cos (2\mu a + \mu_0 a_0) x \cos a_0 y$$

(continued)

$$- \frac{2t^2\mu_0^2a^2a_0^2A_{02}(A_{11}^*+A_{11}^0)}{[(\mu_0a_0)^2+(2a-a_0)^2]^2} \cos \mu_0a_0x \cos (2a-a_0)y$$

$$- \frac{2t^2\mu_0^2a^2a_0^2A_{02}(A_{11}^*+A_{11}^0)}{[(\mu_0a_0)^2+(2a+a_0)^2]^2} \cos \mu_0a_0x \cos (2a+a_0)y \qquad (40)$$

Now, with the introduction of the stress function F, equation (40), and the initial and arbitrary displacements w_0 and w, equations (38) and (39), into equation (17), the total potential energy is obtained, in terms of the displacement amplitude and the buckle wavelength parameters, and it is expressed as

$$U = \left(\frac{\sigma R}{Et}\right)^2 + \frac{\mu^4}{(\mu^2+1)^2}\left(\frac{A_{11}}{2} - \eta A_{11}A_{20} - \eta A_{11}A_{02}\right)^2 + \frac{\mu^4\eta^2}{128} A_{11}^4$$

$$+ \frac{1}{2}\left(A_{20} - \frac{\eta}{8} A_{11}^2\right)^2 + \frac{\mu^4\eta^2A_{11}^2A_{20}^2}{(9\mu^2+1)^2} + \frac{\mu^4\eta^2A_{11}^2A_{02}^2}{(\mu^2+9)^2} + \frac{4\mu^4\eta^2A_{20}^2A_{02}^2}{(\mu^2+1)^2}$$

$$+ \frac{\mu_0^4\eta_0^2}{128}(A_{11}^{*2}+2A_{11}^*A_{11}^0)^2 + \frac{\mu_0^4}{4(\mu_0^2+1)^2}[A_{11}^*-2\eta_0(A_{11}^*A_{20}^*+A_{20}^*A_{11}^0+A_{11}^*A_{20}^0)]^2$$

$$+ \frac{1}{128}[8A_{20}^*-\eta_0A_{11}^*(A_{11}^*+2A_{11}^0)]^2 + \frac{\mu_0^4\eta_0^2}{(9\mu_0^2+1)^2}(A_{11}^*A_{20}^*+A_{20}^*A_{11}^0+A_{11}^*A_{02})^2$$

$$+ \frac{4\mu_0^4\eta_0^2\eta^2}{(\eta_0\mu_0^2+\eta)^2}(A_{02}A_{20}^*+A_{02}A_{20}^0)^2 + \frac{\eta^2\eta_0^2(\mu-\mu_0)^4A_{11}^2(A_{11}^*+A_{11}^0)^2}{64[(\mu\sqrt{\eta}-\mu_0\sqrt{\eta_0})^2+(\sqrt{\eta}-\sqrt{\eta_0})^2]^2}$$

$$+ \frac{\eta^2\eta_0^2(\mu-\mu_0)^4A_{11}^2(A_{11}^*+A_{11}^0)^2}{64[(\mu\sqrt{\eta}+\mu_0\sqrt{\eta_0})^2+(\sqrt{\eta}+\sqrt{\eta_0})^2]^2} + \frac{\eta^2\eta_0^2(\mu+\mu_0)^4A_{11}^2(A_{11}^*+A_{11}^0)^2}{64[(\mu\sqrt{\eta}-\mu_0\sqrt{\eta_0})^2+(\sqrt{\eta}+\sqrt{\eta_0})^2]^2}$$

$$+ \frac{\eta^2\eta_0^2(\mu+\mu_0)^4A_{11}^2(A_{11}^*+A_{11}^0)^2}{64[(\mu\sqrt{\eta}+\mu_0\sqrt{\eta})^2+(\sqrt{\eta}-\sqrt{\eta_0})^2]^2} + \frac{\mu_0^4\eta^2\eta_0^2A_{11}^2(A_{20}^*+A_{20}^0)^2}{[(\mu\sqrt{\eta}-2\mu_0\sqrt{\eta_0})^2+\eta]^2}$$

(continued)

$$+ \frac{\mu_0^4\eta^2\eta_0^2A_{11}^2(A_{20}^*+A_{20}^0)^2}{[(\mu\sqrt{\eta}+2\mu_0\sqrt{\eta_0})^2+\eta]^2} + \frac{\mu^4\eta^2\eta_0^2A_{20}^2(A_{11}^*+A_{11}^0)^2}{[(2\mu\sqrt{\eta}-\mu_0\sqrt{\eta_0})^2+\eta_0]^2}$$

$$+ \frac{\mu^4\eta^2\eta_0^2A_{20}^2(A_{11}^*+A_{11}^0)^2}{[(2\mu\sqrt{\eta}+\mu_0\sqrt{\eta_0})^2+\eta_0]^2} + \frac{\mu_0^4\eta^2\eta_0^2A_{02}^2(A_{11}^*+A_{11}^0)^2}{[\mu_0^2\eta_0+(2\sqrt{\eta}-\sqrt{\eta_0})^2]^2} + \frac{\mu_0^4\eta^2\eta_0^2A_{02}^2(A_{11}^*+A_{11}^0)^2}{[\mu_0^2\eta_0+(2\sqrt{\eta}+\sqrt{\eta_0})^2]^2}$$

$$+ \frac{\eta^2(\mu^2+1)^2A_{11}^2}{48(1-\nu^2)} + \frac{2\eta^2(\mu^4A_{20}^2+A_{02}^2)}{3(1-\nu^2)} + \frac{\eta_0^2(\mu_0^2+1)^2A_{11}^{*2}}{48(1-\nu^2)} + \frac{2\mu_0^4\eta_0^2A_{20}^{*2}}{3(1-\nu^2)} \qquad (41)$$

where $\eta = \pi^2Rt/\lambda_y^2 = a^2Rt$ and $\eta_0 = \pi^2Rt/\lambda_{y_0}^2 = a_0^2Rt$

The first term in equation (41), that is, the average stress, can be expressed in terms of the applied end shortening e and the displacement parameters by utilizing the relation defining the unit end shortening

$$e = -\frac{1}{L}\int_{-L/2}^{L/2} u_{,x}dx \qquad (42)$$

In terms of the stress function F and the displacements, equation (42) becomes

$$e = -\frac{1}{L}\int_{-L/2}^{L/2}[\frac{1}{E}(F_{,yy}-\nu F_{,xx})-(\frac{1}{2}w_{,x}^2+w_{,x}w_{0,x})]dx \qquad (43)$$

by virtue of equation (5), equation (7) written for the middle surface, and equation (16). Substitution of equations (38), (39), and (40) into equation (43) and performance of the indicated operations yields (after multiplication of both sides of equation (43) by R/t)

$$e\frac{R}{t} = \frac{\sigma R}{Et} + \mu^2\eta(\frac{A_{11}^2}{8} + A_{20}^2) + \mu_0^2\eta(\frac{A_{11}^{*2}}{8} + A_{20}^{*2} + \frac{A_{11}^*A_{11}^0}{4} + 2A_{20}^*A_{20}^0) \qquad (44)$$

The variation of the total energy (41) with respect to all of the free parameters yields a set of nonlinear algebraic equations in the variables of the assumed displacement, equation (39), with the prescribed end

shortening being the forcing function. The variation is made independently of A_{00}. This parameter is evaluated by enforcing the periodicity condition on the displacement v. With the use of equation (5), equation (7) written for the middle surface, and equation (16), the relation

$$v,_y = \frac{1}{E}(F,_{xx} - \nu F,_{yy}) - \frac{1}{2} w,_y^2 - w,_y w_{0,_y} + \frac{w}{R} \tag{45}$$

is obtained. When equations (38), (39), and (40) are introduced into (45), the resulting expression yields trigonometric relations in terms of y and additional terms independent of y; hence, these terms are set equal to zero with the result that

$$A_{00} = \eta\left(\frac{A_{11}^2}{8} + A_{02}^2\right) + \frac{\eta_0}{8}\left(A_{11}^{*2} + 2A_{11}^{*}A_{11}^{0}\right) - \nu\frac{\sigma R}{Et} \tag{46}$$

APPENDIX III

SOLUTION OF CURVED-PLATE PROBLEM

The assumed radial deflection shape in the curved plate is assumed to be, in general,

$$w = tA_{11} \cos \frac{\pi x}{\lambda_x} \cos \frac{\pi y}{\lambda_y} + tA_{01} \cos \frac{\pi y}{b} + tA_{21} \cos \frac{2\pi x}{\lambda_x} \cos \frac{\pi y}{\lambda_y} \tag{47}$$

However, in the present solution, the buckle aspect ratio $\mu = \lambda_y/\lambda_x$ is assumed to be unity and $\lambda_y = b/N$, where N is odd and L/b is even.

The corresponding stress function is

$$F = E\left\{-(t^2A_{11}^2/32) \cos \frac{2N\pi x}{b} - \left(\frac{t^2A_{11}^2}{32}\right) \cos \frac{2N\pi y}{b} - \frac{t^2A_{21}^2}{128} \cos \frac{4N\pi x}{b}\right.$$

$$- \frac{t^2A_{21}^2}{8} \cos \frac{2N\pi y}{b} - \frac{t^2A_{11}A_{21}}{4} \cos \frac{N\pi x}{b} - \frac{t^2A_{11}A_{21}}{36} \cos \frac{3N\pi x}{b}$$

$$- \frac{9}{100} t^2A_{11}A_{21} \cos \frac{N\pi x}{b} \cos \frac{2N\pi y}{b} - \frac{t^2A_{11}A_{21}}{676} \cos \frac{3N\pi x}{b} \cos \frac{2N\pi y}{b}$$

$$- \frac{N^2t^2A_{11}A_{01}}{2[N^2+(N-1)^2]^2} \cos \frac{N\pi x}{b} \cos \frac{(N-1)\pi y}{b}$$

$$- \frac{N^2t^2A_{11}A_{01}}{2[N^2+(N+1)^2]^2} \cos \frac{N\pi x}{b} \cos \frac{(N+1)\pi y}{b}$$

$$- \frac{2N^2t^2A_{01}A_{21}}{[4N^2+(N-1)^2]^2} \cos \frac{2N\pi x}{b} \cos \frac{(N-1)\pi y}{b}$$

$$- \frac{2N^2t^2A_{01}A_{21}}{[4N^2+(N+1)^2]^2} \cos \frac{2N\pi x}{b} \cos \frac{(N+1)\pi y}{b} + \frac{b^2tA_{11}}{4R\pi^2N^2} \cos \frac{N\pi x}{b} \cos \frac{N\pi y}{b}$$

(continued)

$$+ \frac{4tb^2 A_{21}}{25RN^2\pi^2} \cos \frac{2N\pi x}{b} \cos \frac{N\pi y}{b} - \frac{\sigma y^2}{2E} \Big\} \tag{48}$$

The mean end shortening is

$$e = -\frac{1}{L} \int_{-L/2}^{L/2} [(\frac{\sigma_x}{E} - \nu \frac{\sigma_y}{E}) - \frac{1}{2} w_{,x}^2] dx = \frac{\sigma}{E} + \frac{N^2\pi^2 t^2}{8b^2} (A_{11}^2 + 4A_{21}^2) \tag{49}$$

The total potential energy, excluding the potential of the applied load since the end shortening is assumed constant for a rigid testing machine, is

$$U = N^4\eta^2 A_{11}^4/64 + 17N^4\eta^2 A_{21}^4/128 + (1/64)(1/169 + 281/25)N^4\eta^2 A_{11}^2 A_{21}^2$$

$$+ (\frac{\sigma R}{Et})^2 + N^4\eta^2 A_{11}^2 A_{01}^2 \beta^2 (1+\delta_{1N})/16 + N^4\eta^2 A_{11}^2 A_{01}^2 \alpha^2/16 + A_{11}^2/16$$

$$+ N^4\eta^2 A_{01}^2 A_{21}^2 \Delta^2 (1+\delta_{1N}) + N^4\eta^2 A_{01}^2 A_{21}^2 \gamma^2 + 4A_{21}^2/25$$

$$+ N^4\eta^2 A_{11}^2 A_{01} A_{21} \Delta\delta_{1N}/4 - N\eta A_{11}^2 A_{21} (-1)^{\frac{N-1}{2}}/5\pi + N^4\eta^2 A_{11}^2 A_{01} A_{21} \beta\delta_{1N}/8$$

$$- N\eta A_{11}^2 A_{21} (-1)^{\frac{N-1}{2}}/4\pi + 9N^4\eta^2 A_{11}^2 A_{01} A_{21} \alpha\delta_{1N}/80 - 3N\eta A_{11}^2 A_{21} (-1)^{\frac{N-1}{2}}/20\pi$$

$$-N^2\eta A_{11}^2 A_{01} \beta/4\pi - N^2\eta A_{11}^2 A_{01} \beta/4\pi(2N-1) - N^2\eta A_{11}^2 A_{01} \alpha/4\pi$$

$$+ N^2\eta A_{11}^2 A_{01} \alpha/4\pi(2N+1) - 8N^2\eta A_{01} A_{21}^2 \Delta/5\pi - 8N^2\eta A_{01} A_{21}^2 \Delta/5\pi(2N-1)$$

$$- 8N^2\eta A_{01} A_{21}^2 \gamma/5\pi + 8N^2\eta A_{01} A_{21}^2 \gamma/5\pi(2N+1)$$

$$- 2(1+\nu)[27N\eta A_{11}^2 A_{21} (-1)^{\frac{N-1}{2}}/800\pi - 3N\eta A_{11}^2 A_{21} (-1)^{\frac{N-1}{2}}/32\pi$$

(continued)

$$- N^2\eta A_{11}^2 A_{01}(\alpha^2+\beta^2)/16\pi - 16N^2\eta A_{01}A_{21}^2(\gamma^2+\Delta^2)/25\pi$$

$$- N^2\eta A_{11}^2 A_{01}\beta^2\phi/16\pi(2N-1) + N^2\eta A_{11}^2 A_{01}\alpha^2\psi/16\pi(2N+1)$$

$$- 16N^2\eta A_{01}A_{21}^2\Delta^2\phi/25\pi(2N-1) + 16N^2\eta A_{01}A_{21}^2\gamma^2\psi/25\pi(2N+1)] \qquad (50)$$

where $\eta = \pi^2 Rt/b^2$

$$\alpha = 1/[N^2+(N+1)^2]$$

$$\beta = 1/[N^2+(N-1)^2]$$

$$\gamma = 1/[4N^2+(N+1)^2]$$

$$\Delta = 1/[4N^2+(N-1)^2]$$

$$\psi = 4N^2 + 4N + 1$$

$$\phi = 4N^2 - 4N + 1$$

$$\delta_{1N} = \begin{cases} 1 & \text{for } N = 1 \\ 0 & \text{for } N \neq 1 \end{cases}$$

The boundary conditions satisfied by the assumed deflection are

$$\left.\begin{aligned} & w = 0 \quad \text{at} \quad y = \pm\, b/2 \\ & \int_{-L/2}^{L/2} \sigma_y\, dx = 0 \\ & \int_{-L/2}^{L/2} \tau_{xy}\, dx = 0 \end{aligned}\right\} \qquad (51)$$

UNCLASSIFIED

Security Classification

DOCUMENT CONTROL DATA - R & D

(Security classification of title, body of abstract and indexing annotation must be entered when the overall report is classified)

1. ORIGINATING ACTIVITY (Corporate author) Stanford University Department of Aeronautics and Astronautics Stanford, California	2a. REPORT SECURITY CLASSIFICATION Unclassified 2b. GROUP

3. REPORT TITLE

ON THE OPTIMUM PROPORTIONING OF STIFFENED CIRCULAR CURVED PLATES AND SHELLS FOR AXIAL COMPRESSION LOADING

4. DESCRIPTIVE NOTES (Type of report and inclusive dates)

Final Report

5. AUTHOR(S) (First name, middle initial, last name)

Eli Meller and Jean Mayers

6. REPORT DATE March 1970	7a. TOTAL NO. OF PAGES 70	7b. NO. OF REFS 33
8a. CONTRACT OR GRANT NO. DAAJ02-68-C-0035 b. PROJECT NO. Task 1F162204A17002 c. d.	9a. ORIGINATOR'S REPORT NUMBER(S) USAAVLABS Technical Report 70-9 9b. OTHER REPORT NO(S) (Any other numbers that may be assigned this report)	

10. DISTRIBUTION STATEMENT

This document is subject to special export controls, and each transmittal to foreign governments or foreign nationals may be made only with prior approval of U. S. Army Aviation Materiel Laboratories, Fort Eustis, Virginia 23604.

11. SUPPLEMENTARY NOTES	12. SPONSORING MILITARY ACTIVITY U.S. Army Aviation Materiel Laboratories Fort Eustis, Virginia

13. ABSTRACT

An investigation is undertaken to (1) reevaluate the elastic theory results obtained by previous investigators for both perfect and initially imperfect, axially compressed circular cylindrical shells, (2) develop new elastic stability results describing the postbuckling behavior of curved plates, and (3) present criteria based, in part, upon the curved plate results which can be used to size and locate stringers and rings such that the initial buckling load will occur in the neighborhood of the classical buckling load for a cylinder representing a minimized-weight design.

DD FORM 1 NOV 65 1473 REPLACES DD FORM 1473, 1 JAN 64, WHICH IS OBSOLETE FOR ARMY USE.

UNCLASSIFIED

Security Classification

UNCLASSIFIED
Security Classification

14. KEY WORDS	LINK A ROLE	LINK A WT	LINK B ROLE	LINK B WT	LINK C ROLE	LINK C WT
Curved Plates						
Shells						
Stability						
Postbuckling						
Stiffened Shells						
Optimization						

UNCLASSIFIED
Security Classification